Die approbierte Originalversion dieser Diplom-/Masterarbeit ist an der Hauptbibliothek der Technischen Universität Wien aufgestellt (http://www.ub.tuwien.ac.at).

The approved original version of this diploma or master thesis is available at the main library of the Vienna University of Technology (http://www.ub.tuwien.ac.at/englweb/).



MASTERARBEIT

Fluence measurement at the neutron time of flight experiment at CERN

ausgeführt am

Atominstitut der österreichischen Universitäten

unter der Anleitung von
Univ.Prof. Dr.techn. Gerald Badurek
Dr.techn. Erwin Jericha

durch

Christina Weiß
Kohlgasse 9/13
1050 Wien

Wien, im Mai 2010

Weiß Christina

Contents

1 Introduction **4**

2 The n_TOF facility at CERN **5**

2.1 The aim of n_TOF . . . 5

2.1.1 Astrophysical considerations . . . 5

2.1.2 Nuclear waste . . . 8

2.2 Description of the facility . . . 10

2.3 Spallation target . . . 11

2.4 Time-energy relation . . . 13

3 Neutron physics **15**

3.1 Properties of the neutron . . . 15

3.2 Interactions and cross section . . . 16

3.2.1 Thermal neutron scattering . . . 18

3.2.2 Neutron scattering by a system of bound atoms . . . 21

3.2.3 Spin dependency . . . 22

4 Neutron fluence **24**

4.1 Theory . . . 24

4.2 Fluence measurements at the n_TOF commissioning 2009 . . . 26

4.2.1 Flux measurement using the Micromegas detector . . . 26

4.2.2 Flux measurement using the silicon monitor . . . 28

4.2.3 The double foil method . . . 29

4.2.4 The saturated resonance method . . . 30

5 Fission chamber **32**

5.1 Chamber design . . . 32

5.2 Mode of operation . . . 32

5.3 ^{235}U chamber data . . . 33

5.3.1 Nuclear reactions and fission products . . . 34

5.4 Experimental setup . . . 36

5.4.1 Materials in the experimental setup . . . 37

6 Data analysis **38**

6.1 Experimental data . . . 38

6.2 Background . . . 40

6.3 Corrections for the materials present . . . 42

6.3.1 Air . . . 42

6.3.2 Al window . . . 43
6.3.3 Air within the radiation shielding . . . 45
6.3.4 Ta window . . . 46
6.3.5 Multilayer structure of the fission chamber . . . 46
6.4 Neutron fluence . . . 49
6.5 Results . . . 52
6.6 Results from different detectors . . . 55
6.7 Neutron fluence, old versus new target . . . 57

7 Experiment on neutron absorption in air **59**
7.1 Experimental setup . . . 59
7.2 Calculation of the transmission . . . 61
7.3 Results . . . 62

8 Summary **64**
8.1 Neutron fluence at n_TOF 2009 . . . 64
8.2 Experiment on neutron absorption in air . . . 65

9 Appendix **72**
9.1 Error calculations . . . 72
9.1.1 Error propagation . . . 72
9.1.2 Scattering cross section . . . 73
9.2 Experimental data, neutron transmission experiment with air . . . 76
9.3 Programs, n_TOF data analysis . . . 81
9.3.1 Collecting experimental TOF data . . . 81
9.3.2 Converting TOF to neutron energy . . . 83
9.3.3 Collecting ENDF data . . . 86
9.3.4 Calculation of the reaction yield . . . 91
9.3.5 Calculating the neutron fluence . . . 94
9.3.6 Function for adding the data . . . 97
9.3.7 Function for calculating the number of protons per run . . . 98
9.3.8 Function for data linearisation . . . 99
9.3.9 Function for histogram binning . . . 101

1 Introduction

At the neutron time of flight facility n_TOF at CERN a new spallation target was installed in 2008. In 2008 and 2009 the commissioning of the new target took place. During the summer 2009 a fission chamber of the Physikalisch Technische Bundesanstalt (PTB) Braunschweig was used for the neutron fluence measurement.

The evaluation of the data recorded with this detector is the primary topic of this thesis.

Additionally a neutron transmission experiment with air has been performed at the TRIGA Mark II reactor of the Atomic Institute of the Austrian Universities (ATI). The experiment was implemented to clarify a question about the scattering cross section of molecular gas which could not be answered clearly via the literature. This problem came up during the evaluations for n_TOF.

2 The n_TOF facility at CERN

2.1 The aim of n_TOF

The neutron time of flight facility n_TOF at CERN, Geneva/Switzerland, was built to determine neutron cross sections σ, which are specific to each isotope and reaction and are dependent on the neutrons energy. This quantity is of high interest in nuclear physics. The resonance structure of the cross sections allow, for example, to investigate nuclear energy levels.
In astrophysics the data is needed to understand the processes which are responsible for the nucleosynthesis of elements heavier than Fe.
The not insignificant problem of nuclear waste led to the development of Accelerator Driven Systems (ADS) for the incineration of the radio-toxic materials produced in nuclear reactors. For the design and understanding of the behavior of ADS, which can also be used for energy production and radio-isotopic activation for medical and other applications, an accurate knowledge of the nuclear cross sections is required.

2.1.1 Astrophysical considerations

One of the major interests in astrophysics is to understand the natural abundances of the elements and their isotopes in our solar system and generally in our universe, known through investigations of our sun, meteorites and astronomical research. Associated with this question are the creation mechanisms for all, stable and unstable, isotopes. With a few exceptions, all nuclides are synthesized in stars.
In the *chart of nuclides*, see Fig. 1, all the known isotopes are mapped, together with additional information like their half life, natural abundance or nuclear energy levels. On the vertical axis the number of protons, on the horizontal axis the number of neutrons per nucleus is displayed.
One of the primary properties of an isotope is it's half life $t_{1/2}$, which is defined as the time it takes for a given amount of the isotope to decrease by half through radioactive decay. As the radioactive decay follows an exponential law, the half life is a constant value for each isotope.
Non-radioactive nuclides are called stable. These isotopes form the valley of stability in the chart of nuclides. Isotopes on either sides of this valley and isotopes with more than 82 protons will undergo radioactive decay of some sort in order to reach the valley of stability. Most of the naturally occurring nuclides are stable. There are a few more isotopes that have a half-life greater or equal to the earth's age (4.5 billion years). These can also be

found in nature. An example of naturally occurring radioactive nuclides are ^{235}U, with a half life of $7.04 \cdot 10^8$ years, and ^{238}U, with $t_{1/2} = 4.468 \cdot 10^9$ years.

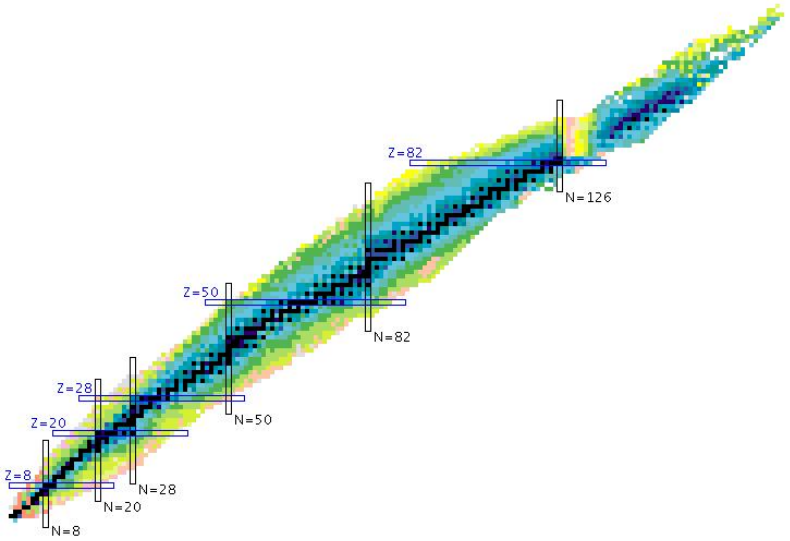


Figure 1: Chart of nuclides, after [1]. The colour code indicates the different half lives of the isotopes. Isotopes with a half life greater than 10^{15} seconds are marked in dark blue. Up to the mark of 82 protons and 126 neutrons the so called "valley of stability" follows this dark blue line.

The main constituent of all luminous matter in the universe is ^{1}H and ^{4}He with 71.1% and 27.4% respectively [2]. The natural abundance of the other nuclides shows a peak at ^{12}C and ^{16}O and at the atomic mass numbers $A = 50 - 65$ at the so called "iron peak". In general the abundance drops slowly with increasing mass number. The more precise distribution of the natural abundances shows a dependency of the individual numbers of nucleons, which is a reference to the shell structure of the atomic nucleus.

The nuclides below the iron peak are created in various stellar burning phases. Nuclear reactions induced by charged particles, such as protons or α particles, are responsible for their creation. Only Li, Be and B seem to underlie an extra solar mechanism as they can easily be destroyed in fusion reactions using charged particles.

Beyond the nuclides of the iron peak, which represent the most stable isotopes, the large Coulomb repulsion makes a charged particle-induced reaction unlikely. The heavier isotopes are therefore created via the neutron capture reaction (n,γ).

The slow neutron capture process, s-process, occurs in the solar burning phases. In these environments the neutron number density is small so that the decay constant τ_β of the β^- decay is much smaller than the one of the (n,γ) reaction $\tau_{n\gamma}$. The seed nucleus captures a neutron and produces the isotope of the same element with (A+1) nucleons. If this isotope is unstable, meaning radioactive, a subsequent β^- decay converts a neutron into a

proton and an isotope of the next element with N-1 neutrons is formed. The s-process will always run along the valley of stability. Neither neutron-deficient nor neutron-rich stable nuclides can be reached through this process. In Fig. 2 the solid line shows the path of the s-process, starting from the isotope ^{156}Gd. Neither ^{160}Gd nor ^{158}Dy, which are both stable nuclides, can be synthesized via the s-process.

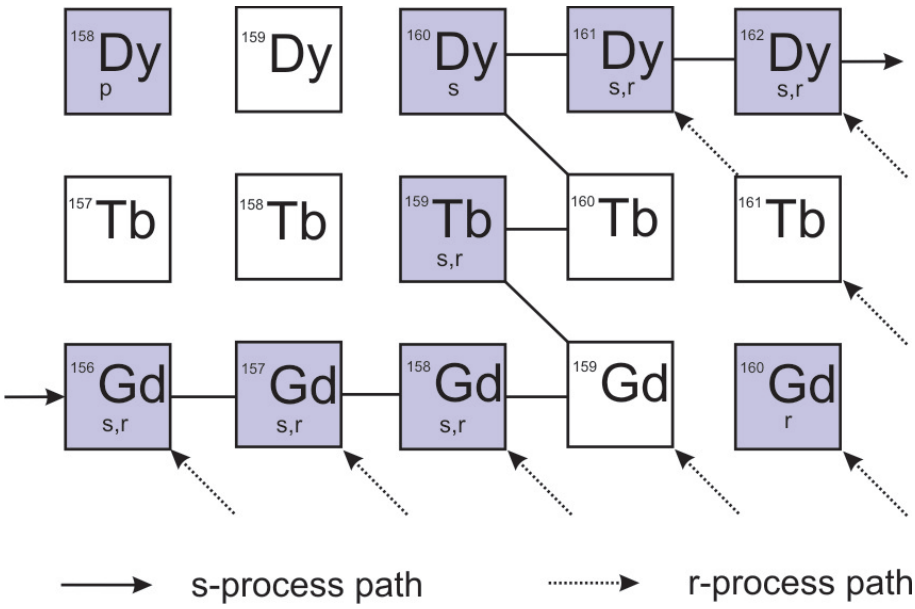


Figure 2: Zoom into the chart of nuclides. The s-process path is shown with solid lines, the r-process with dotted lines. Indicated below each stable isotope is the process responsible for it's creation.

A rough estimate of the number densities of neutrons [2] shows that the s-process happens in environments where typically 10^8 neutrons per cm^3 are available.
When $\tau_\beta \gg \tau_{n\gamma}$ applies, then the rapid neutron capture process, r-process, occurs. Nuclides which are very neutron rich can be produced in environments where a neutron density of 10^{21} and more neutrons per cm^3, like in Type II supernovae, is available. When the neutron flux terminates, the neutron-rich radioactive nuclei will undergo successive β^- decays until a stable nuclide is reached. In Fig. 2 the dashed arrows show the nuclides that can be produced through the r-process.
There are a number of stable nuclides which cannot be reached by either of the two neutron capture processes. Theses nuclides are shielded by other stable nuclides from these processes and are referred to as p-nuclei due to their small number of neutrons. Their abundance is much smaller in comparison with s- and r-nuclei of the same mass number. A significant property of the p-nuclei is that they almost all have an even number of protons and neutrons. The p-process seems to favor the production of paired nucleons and therefore strongly bound nuclei. The (p,γ) and (γ,n) reactions allow the production of

neutron-deficient nuclei.
As an example for a p-nuclide ^{158}Dy is shown in Fig. 2. Neither the s- nor the r-process can synthesize this isotope.

2.1.2 Nuclear waste

Nuclear waste is material that contains radioactive nuclei. Being the product of a nuclear reaction, used for various purposes, it needs to be dealt with carefully as it represents a danger for both human beings and their environment. Power generation as well as nuclear weapons reprocessing produce the majority of nuclear waste. There are also other sources, such as medical applications and industrial processes.
Nuclear waste can be classified from "low-level waste", meaning it contains low levels of radioactivity per mass or volume, up to "high-level waste". The half life of each of the produced isotopes plays a predominant role in the management of these radiotoxic materials.
In many countries a once-through fuel cycle predominates. Spent fuel is accumulated in spent fuel storage pools and intermediate storage facilities. As radioactivity, by definition, reduces over time, the primary approach is to isolate the dangerous material. For long-lived waste this becomes a fundamental problem.
Some countries developed a reprocessing fuel cycle. Plutonium and Uranium get separated and can be reused as fuel in light water reactors (LWR), the most common reactors in use for nuclear power stations. But the not insignificant remaining mix of minor actinides and fission products creates all the same a problem of final waste disposal.
Nuclear waste transmutation has been proposed for reducing substantially the inventory of the long lived component of the waste. Mainly the trans-uranium actinides, isotopes of U, Np, Pu, Am, Cm and higher Z actinides, should be transmutated by fission in *Fast Critical Reactors* or subcritical *Accelerator Driven Systems* (ADS). For the proper design, safety regulation and precise performance assessment of transmutation devices, accurate and reliable neutron capture cross section data is needed.
As the fuel utilization in LWR is as little as 1% of the total deployed fuel, additional strategies are needed in order to reduce the nuclear waste problem. Combining the operation of fast reactors, where Plutonium is employed as fuel, and the transmutation strategy could lead to a more satisfying outcome than current procedures.
The *Integral Fast Reactor* (IFR) concept, where Plutonium as well as the minor actinides present in the nuclear waste could serve as fuel, would be the most economic strategy in fuel utilization and radiotoxicity reduction [3].
Fast neutron reactors are nuclear reactors where fast neutrons sustain the fission chain

reaction. Contrary to slow neutron reactors, the fast reactor does not need a moderator. On the other side it needs a fuel that is relatively rich in fissile material. There is also the possibility of producing fuel within a fast reactor which is implemented in so called "fast breeding reactors".
The advantage of nuclear reactions induced by fast neutrons is that, at these energies, the fission cross section of actinides is often higher than the capture cross section, as can be seen in Fig. 3 using the example of ^{239}Pu. This gives an advantage in the transmutation of nuclear waste.

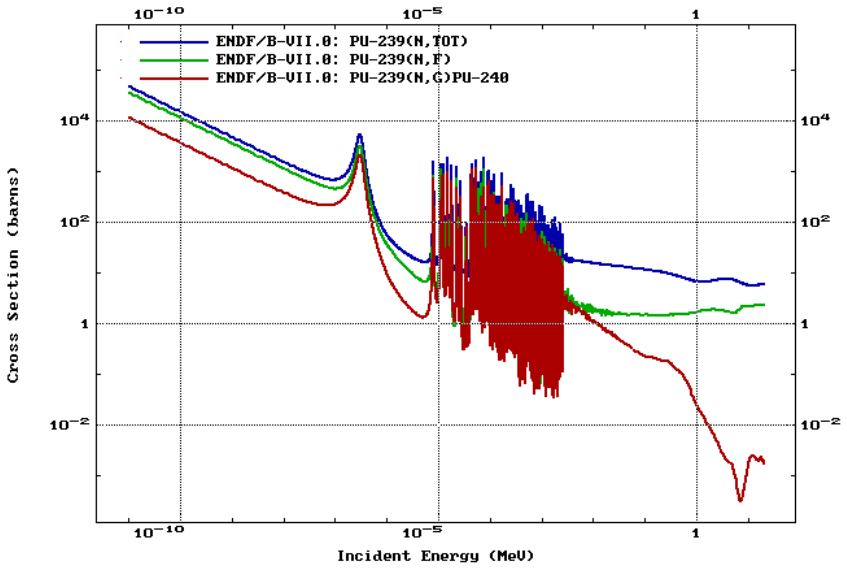


Figure 3: Cross sections of ^{239}Pu against the energy of the incident neutrons, after [1]. The fission cross section is drawn in green, the capture cross section in red. The blue curve, approximately the sum of the two, is the total cross section of ^{239}Pu.

Most of the scenarios for ADS are proposed with fuel highly enriched with trans-uranium actinides and the use of fast neutron spectra. ADS are nuclear fission reactors which have an external neutron source, preferably a particle accelerator producing neutrons by spallation. These reactors are run subcritically, which gives a big advantage on safety considerations.

2.2 Description of the facility

The n_TOF facility was build after the concept of Carlo Rubbia et al. [4] into an existing proton beam dump tunnel at the Proton Synchrotron (PS). The motivation was to provide a neutron time of flight facility with a very high neutron flux, allowing the analysis of samples with very modest mass of normally less than 1 gram, and a neutron spectrum over a very wide energy range, namely from thermal energies up to 250 MeV.
Additionally the excellent calculated energy resolution $\frac{\Delta E}{E} \approx 3 \cdot 10^{-3}$ assured a good resolution of the resonances found in the cross sections, which are of primary interest for nuclear physics.

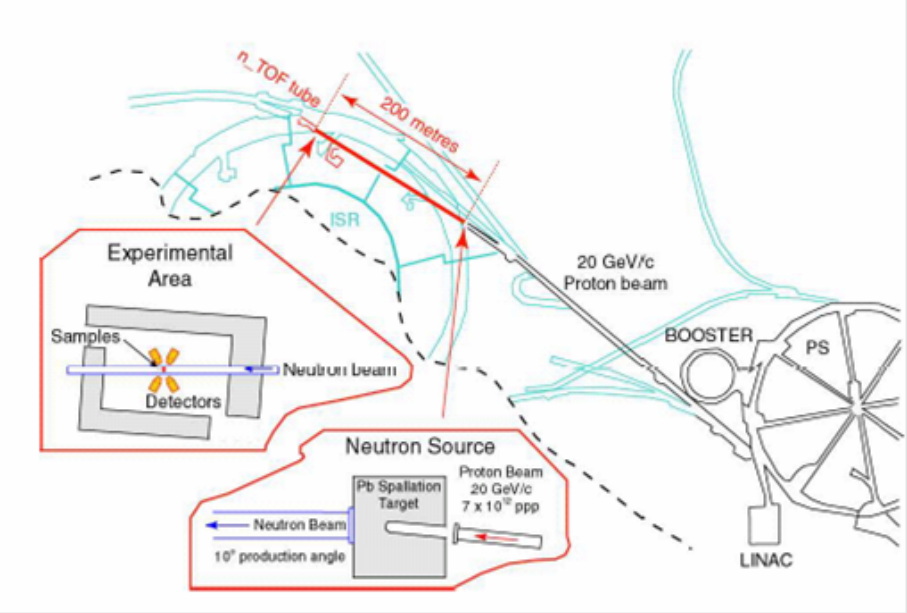


Figure 4: n_TOF facility layout at CERN.

The neutron beam is created by protons hitting a spallation target made of lead. The protons, accelerated by the PS to 20 GeV/c, arrive on average every 2.4 seconds at the target as dedicated or parasitic pulses of intensity $7 \cdot 10^{12}$ and $4.5 \cdot 10^{12}$ protons/pulse respectively. The proton pulse width is 6 ns root mean square (rms).
When leaving the spallation target the created neutrons get moderated by a 5 cm thick layer of H_2O before they enter the TOF tube through an Al window. The flight path is inclined by 10° with respect to the incident proton beam axis as can be seen in Fig. 4 (cut-out: Neutron Source). This is to avoid the forward shower of particles and photons at 0°. The TOF tube is in total 200 m long and evacuated to a pressure of 10^{-3} bar.
The spallation process produces, apart from the required neutrons, various other charged and uncharged elementary particles. Most of them are unstable, with a lifetime much

shorter than the TOF range, and therefore do not reach the experimental area. The γ rays are "prompt" and provide the needed t=0 calibration as will be mentioned in Sec. 2.4. Through the TOF measurement they can easily be distinguished from the fastest neutrons with about 250 MeV energy.
The neutron beam gets progressively reduced from 80 cm to 60 cm and finally to 40 cm before a first collimator located about 136 m from the spallation target. The inner diameter of this 1 m long collimator, which is made of iron and concrete, is about 11 cm.
Massive concrete and iron shieldings are situated at about 72 and 140 m.
At 145 m a sweeping magnet is installed which removes the charged particle background, consisting primarily of electrons and pions, but also protons, kaons and muons, from the neutron beam. As a strong muon background was detected at the experimental area during the first commissioning of the facility, a muon shielding made of concrete and iron sections, each 3 m in thickness, was placed at the sweeping magnets location.
A second collimator made out of borated polyethylene and iron is placed at 176 m. This collimator can be installed with an inner diameter of 1.8 cm for capture or 8 cm for fission cross section measurements.
In capture cross section measurements the emitted γ rays from the (n,γ) reaction get detected. The sample's thickness is therefore not a critical value and small thick samples can be used. The inner diameter of the second collimator of 1.8 cm is sufficient to cover the area of the samples in use.
When measuring the fission cross section the fission products of the (n,f) reaction must be detected. This requires very thin samples in order to reduce the absorption of the fission products in the sample itself. For realistic experimental periods a large surface of the samples is required to get a significant number of fission events. Therefore the second collimator needs to be installed with the larger inner diameter when performing fission cross section measurements.
The experimental area starts at 182.5 m where 7.5 m are reserved for the measuring station. The neutrons flight path ends in the 10 m long escape lane, which acts as a beam dump.

2.3 Spallation target

Natural lead was taken as the material for the spallation target as it has a high neutron yield ($\approx$ 30 n/proton at 1 GeV) which is linearly growing for higher energies and is nearly transparent for neutrons with energies $\leq$ 1 MeV. With the proton energy of 20 GeV at the Cern PS, about 300 neutrons get produced by an incident proton.
In 2004 an abnormal increase of the radioactivity in the water of the target cooling system was observed. Based on considerations for radio protection it was decided to replace the

old target by a new spallation target with modified geometry.
The new spallation target, see Fig. 5, consists of a cylindrical Pb block, 60 cm in diameter and 40 cm in length, cooled by a forced flow of water. The target and the water, enclosed in an Al container, was installed in the old target container.

By defocussing the incident proton beam and through the forced cooling water flow, it is guaranteed that the water temperature does not reach the boiling point and that the temperature inside the target stays well below the Pb melting point.
A very thin Al window is installed in the forward direction, after a 5 cm thick water layer which acts as cooling for the target and as moderator for the neutrons. The cooling layer of 1 cm thickness is separated from the moderator layer of 4 cm thickness. The fluid used for moderation can be exchanged and it is planned to insert borated water at a later date. At the commissioning and the experimental phase in 2009 water was used as moderator.
The subject of this thesis is the neutron fluence measurement at the commissioning of the new spallation target at n_TOF which took place in summer 2009. The parameters of the facility which had to be determined at the commissioning were the following:

- Neutron fluence distribution
- Neutron beam profile
- Neutron energy resolution function
- Time-energy relation
- Background

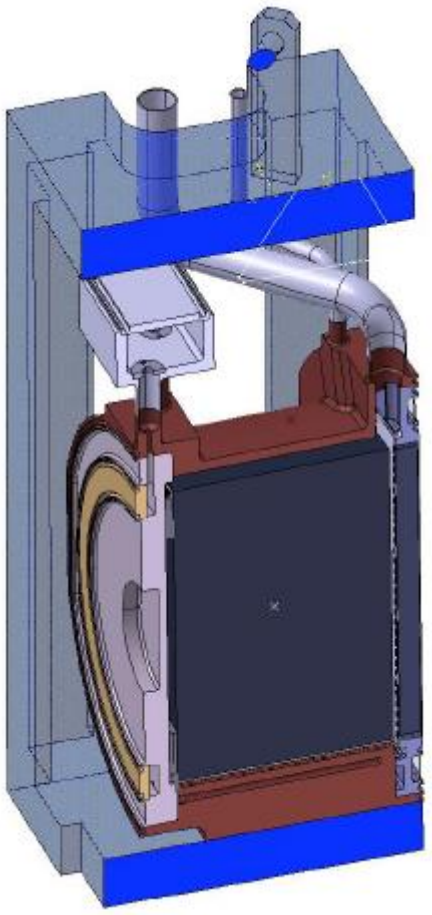


Figure 5: Cut through a model of the new spallation target at the n_TOF facility, after [5].

2.4 Time-energy relation

At a TOF experiment the detection time t_{det} of the particles gets measured and converted into the time t they needed to travel a given distance L.

$$t \;=\; t_{det} \;-\; t_{pkup} \;-\; t_{\gamma} \;+\; t_{light} \tag{1}$$

Where t_{pkup} is the time at which the protons arrived at the spallation target, t_{γ} is the detection time of the prompt γ-rays at the experimental area and t_{light} is the time that light needs for travelling the given distance of the experiment.
In the case of neutrons with mass m_n, this time is related to the energy of the neutrons E_n through the classical relationship:

$$E_n \;=\; \frac{1}{2}\, m_n\, v^2 \;=\; \left(\frac{72.2977\; L}{t}\right)^2 \tag{2}$$

Where the neutron energy E_n is given in [eV], the flight path L in [m] and the time of flight t in [μs]. The non-relativistic calculation is valid in the energy range of interest (0-20 MeV).
Due to the creation process of the neutrons in the lead target, their moderation in the cooling water and the time distribution of the initial proton pulse [6], the flight path L is defined by the geometrical flight path L_0 and an additional length ΔL. ΔL is dependent on the neutron energy and accounts for the neutrons path in the lead target and the subsequent moderation process in the cooling water.

$$L(E_n) \;=\; L_0 \;+\; \Delta L(E_n) \tag{3}$$

It can be demonstrated [7] that this is equivalent to a constant time offset t_0. Substituting L in Eq. 2 leads to

$$E_n \;=\; \left(\frac{72.2977\; (L_0 + \Delta L(E_n))}{t}\right) \;=\; \left(\frac{72.2977\; L_0}{t \;+\; t_0}\right). \tag{4}$$

In order to find the calibration parameters, a set of standard resonances have been measured at n_TOF [7]. According to these measurements the correction for the length of the flight path in meters is

$$\Delta L \;=\; (0.094 \pm 0.018) \cdot 10^{-2}\; \sqrt{E_n}. \tag{5}$$

This is equivalent to a time offset of $t_0 = -(68 \pm 13)$ ns.
The values of ΔL and t_0 respectively is dependent on the spallation target's geometry and the thickness of the water layer. The given values were determined for the old spallation target. The observable resonances of the materials in the experimental data of the fluence

measurement, see Sec. 6, indicate that the calibration parameters are valid also for the new target.

3 Neutron physics

3.1 Properties of the neutron

The neutron is an elementary particle. Neutrons and protons, as they are the constituents of the atomic nucleus, are collectively referred to as nucleons. The number of protons in a nucleus is known as the atomic number Z, the number of neutrons is called the neutron number N. The sum of the two is called the mass number A. The following notations for atomic nuclei are valid.

$$(A, Z), \qquad {}^{A}X, \qquad {}^{A}_{Z}X, \qquad {}^{A}_{Z}X_{N}.$$

The notation used in this thesis will always be the second, for example ^{235}U for the uranium isotope with 143 neutrons.
The properties of the particles which compose the atom are listed in the following table.

Particle	Charge q	Spin	Mass
Neutron	$q = 0$	$\frac{1}{2}$	939.5657 MeV
Proton	$q = +e_0$	$\frac{1}{2}$	938.2724 MeV
Electron	$q = -e_0$	$\frac{1}{2}$	0.510999 MeV

For practical reasons, neutrons are classified according to their kinetic energy. The divisions occur as a result of the interactions peculiar to certain ranges of energy. The most commonly used terms are listed below [8].

- Cold Neutrons: Are neutrons who's wavelength $\lambda = \frac{h}{mv}$, where h is Planck's constant and mv is the momentum of the neutron, is big enough to still be reflected by a crystal. After Bragg's law

  $$n\lambda \;=\; 2d\sin\Theta$$

  this is the case for $\lambda > 2d$, with d the lattice spacing of the crystal. The energy range of these neutrons is 0 - 0.002 eV.

- Thermal Neutrons: The average energy of the neutrons is equal to the average thermal energy of the atoms of the medium. The velocity distribution of the neutrons approaches the Maxwell distribution

  $$\mathrm{d}n(v) \;=\; Av^2 e^{-m_n v^2/2kT}\mathrm{d}v, \tag{6}$$

where v is the velocity of the neutron, m_n its mass, k Boltzmann's constant and T the absolute temperature. At room temperature the maximum number of neutrons will have an energy of approximately 0.025 eV.

- Epithermal Neutrons: The neutrons have an average energy from 0.025 eV up to 1 eV.
- Resonance Neutrons: Neutrons in the energy range of 1-100 eV get strongly absorbed by various nuclei. These reactions happen at fairly well defined energies. The typical structure in the cross section data of the isotopes is called the resonance region.
- Intermediate Neutrons: These are neutrons in the energy region between 100 eV and 0.5 MeV.
- Continuum Region Neutrons: Neutrons with an energy higher than 0.01 MeV are sometimes called continuum region neutrons. Notations like high-energy and ultra-high-energy neutrons can be found in the literature. However, in this high energy region the classification is not as specially defined as it is for slower neutrons.

3.2 Interactions and cross section

The neutron underlies the strong, weak, electromagnetic and gravitational interaction. The electromagnetic interaction is due to the magnetic moment caused by the spin of the neutron. Due to the absence of a charge it does not underlie the Coulomb interaction.
In contrary to bound neutrons, free neutrons are unstable and undergo β decay with a half life of $t_{1/2} = (613.9 \pm 0.6)$ s [1].

$$n \rightarrow p^+ + e^- + \overline{\nu}_e \tag{7}$$

To describe the interaction of the neutron with other matter the *cross section* σ was introduced. When J is a flux of neutrons in an incident collimated beam and N the number of atoms exposed to this beam, then the rate, r, at which a particular type of interaction occurs can be written as

$$r = J\sigma N. \tag{8}$$

Obviously σ is the probability for the interaction and has the unit of an area. In nuclear physics σ is usually given in barn, where 1 barn = 10^{-28} m^2. A cross section for various interactions can be specified, for instance for scattering or absorption. The sum of all possible interactions gives the total cross section σ_{tot}, meaning the probability for a specific

material of having any kind of interaction with a neutron.

$$\sigma_{tot} \;=\; \sum_i \sigma_i \tag{9}$$

As the number of atoms N are changed from their original state through the interaction with the neutrons, r in Eq. (8) can be written as $-\frac{\mathrm{d}N}{\mathrm{d}t}$ which gives the differential equation [8]

$$\frac{\mathrm{d}N}{\mathrm{d}t} \;=\; -nv\sigma N. \tag{10}$$

Here n is the number of neutrons with velocity v in the beam. Integration of this relation yields the number of atoms N in the original state at the time t.

$$N(t) \;=\; N(t_0)e^{-nv\sigma t} \tag{11}$$

In order to find the number of neutrons being removed from the incident beam through the interaction with the present material, the area A of the beam has to be compared with the cross-sectional area of the target atoms. In a target of thickness x with N atoms per cm^3, NAx atoms get exposed to the beam. Their cross-sectional area is therefore $NAx\sigma$. As the number of neutrons removed from the incident beam is $NAx\sigma/A$, the corresponding number for the path $\mathrm{d}x$ is

$$\frac{\mathrm{d}n}{n} \;=\; -N\sigma\mathrm{d}x, \tag{12}$$

which gives, on integration, the number of neutrons in the beam after transversing the layer of thickness x.

$$n(x) \;=\; n(0)e^{-\Sigma x} \qquad \text{where} \qquad \Sigma \;=\; N\sigma \tag{13}$$

The quantity Σ is called the macroscopic cross section and has the dimension cm^{-1}. The relation between Σ and the mean free path λ_{tot} of the neutrons in a material is given by the relation

$$\lambda_{tot} \;=\; \frac{1}{\Sigma_{tot}}. \tag{14}$$

All possible interactions of the neutron with the atoms in the target are accounted for in this relation.

If the beam passes through a material with molecules composed by isotopes with differing cross sections Eq. (8) becomes

$$r \;=\; JN_{mole}\sum_i n_i\sigma_i, \tag{15}$$

wherein

$$N_{mole} \;=\; \frac{\text{density}}{\text{molecular weight}} \cdot \text{Avogadro constant} \tag{16}$$

represents the number of molecules in a cm^3 and n_i is the number of atoms with the cross section σ_i within the molecule [9].
The cross sections σ_i, and therefore also Σ, are characteristic for each isotope and reaction. σ_i stands for the probability of a neutron interacting in a certain way i with an atom of the given isotope.
In principle the total cross section from relation (9) can be written as

$$\sigma_{tot} \;=\; \sigma_s + \sigma_a. \tag{17}$$

Neutrons get either scattered, σ_s, or absorbed, σ_a, by the nuclei within the present material. If a mixture of isotopes is given, with fractions of isotopes of type i and $\sum_i C_i = 1$, then the scattering and absorption cross sections become

$$\sigma_s \;=\; \sum_i C_i \sigma_{si} \qquad\qquad \sigma_a \;=\; \sum_i C_i \sigma_{ai}. \tag{18}$$

3.2.1 Thermal neutron scattering

For the theoretical description of the scattering of a neutron with mass m by a nucleus with mass M, the Schrödinger equation has to be solved. In position space it has the form

$$\left[-\frac{\hbar^2}{2m}\Delta + V(\vec{r}) \right] \Psi_{\vec{k}}(\vec{r}) \;=\; E_k \Psi_{\vec{k}}(\vec{r}). \tag{19}$$

In order to describe both, the scattering and the absorption, $V(\vec{r})$ is taken as a complex optical potential to represent the effective interaction between the neutron and the nucleus. This optical potential represents the short-range strong interaction which is by far the most important interaction in nonmagnetic materials.
For thermal neutrons only s-wave scattering is appreciable so that $V(\vec{r})$ can be taken as central potential [10]. The asymptotic behavior of the resulting wave function is a superposition of the incident plane wave and an outgoing spherical wave.

$$\Psi_{\vec{k}}(\vec{r}) \;\overset{r\to\infty}{\longrightarrow}\; (2\pi)^{-3/2} \left[\underbrace{\exp(i\vec{k}\vec{r})}_{\text{plane wave}} - f(\Theta) \underbrace{\frac{\exp(ikr)}{r}}_{\text{spherical wave}} \right] \tag{20}$$

The amplitude $f(\Theta)$ of the scattered wave is determined by the matrix element of the *transition operator* T between the initial and final states, which describes the interaction.

$$f(\Theta) \;=\; -\frac{4\pi^2 m}{\hbar^2}\,\langle\vec{k}'|\,T\,|\vec{k}\rangle \;=\; \langle\vec{k}'|\,F\,|\vec{k}\rangle \tag{21}$$

The quantity $F = -\frac{4\pi^2 m}{\hbar^2}\,T$ is called the *scattering amplitude operator*.
Through the optical theorem the total cross section is related to the imaginary part of the scattering amplitude in forward direction.

$$\sigma_{tot} \;=\; \frac{4\pi}{k}\,\Im[f(0)] \tag{22}$$

For thermal neutrons a series expansion can be made

$$f(\Theta) \;=\; -a + ika^2 + O(k^2), \tag{23}$$

where $a \in \mathbb{C}$ is called *scattering length* which is a characteristic property of the optical potential. This quantity is treated as a phenomenological constant and is determined by the experiment.
Using the optical theorem and the series expansion for the scattering amplitude with $a = a' - ia''$ the following relations for the cross sections are a good approximation [10] for practical purposes:

$$\sigma_{s0} \;=\; 4\pi|a|^2 \tag{24}$$

$$\sigma_{a0} \;=\; \tfrac{4\pi}{k_0}a'' \tag{25}$$

The above results for the cross sections are valid when calculating the scattering of the thermal neutron in the center of mass system, indicated by the subscript 0, by a free atom. When changing into the laboratory system the *bound scattering length* b gets introduced.

$$b \;=\; b' - ib'' \;=\; \left(\frac{A+1}{A}\right)a \tag{26}$$

The relations for the cross sections in the laboratory system become

$$\sigma_s \;=\; 4\pi\eta|a|^2 \tag{27}$$

$$\sigma_a \;=\; \tfrac{4\pi}{k}b''. \tag{28}$$

The factor η is defined as the fraction between the incident fluxes in the two coordinate systems. With the incident neutron number density ϱ and the reduced mass $m_0 = \frac{Mm}{M+m}$

$$\text{Laboratory system:} \qquad J \;=\; \varrho\,\frac{\hbar k}{m} \tag{29}$$

$$\text{Center of mass system:} \qquad J_0 \;=\; \varrho\,\frac{\hbar k_0}{m_0} \tag{30}$$

Hence the factor η in Eq. (27) becomes

$$\eta = \frac{J_0}{J} = \frac{mk_0}{m_0 k} = \left(\frac{A+1}{A}\right)\frac{k_0}{k}. \tag{31}$$

For a gas with n_a atoms in thermodynamic equilibrium at temperature T the cross sections are of the form

$$\begin{aligned} \sigma_s &= 4\pi n_a \langle\eta\rangle |a|^2 \\ &= 4\pi n_a \left(1 + \frac{k_B T}{2AE_{\vec{k}}}\right)|a|^2 \end{aligned} \tag{32}$$

$$\sigma_a = \frac{4\pi n_a}{k} b''. \tag{33}$$

After relation (24) a constant value for σ_s in the low energy region would be expected. In Fig. 6 the cross sections of ^{14}N, as given by the ENDF/B-VII.0 database, are drawn. The increase of σ_s in the low energy area can be understood through relation (32). The "$1/v$ law" in σ_a is clearly visible up to an energy of about 0.1 MeV.

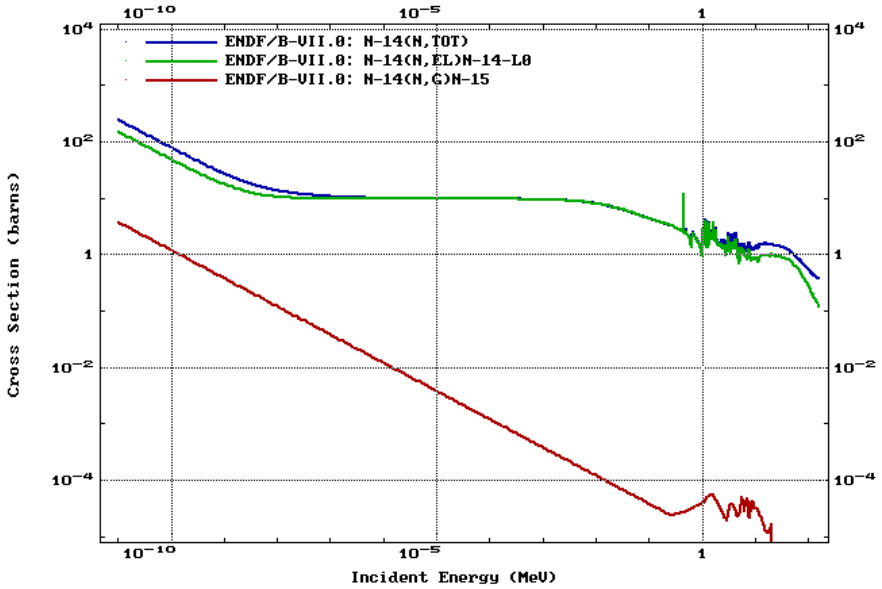


Figure 6: Cross sections of ^{14}N against the energy of the incident neutrons, after [1]. The scattering cross section σ_s is drawn in green, the capture cross section σ_a in red. The blue curve is the total cross section σ_{tot} of ^{14}N.

3.2.2 Neutron scattering by a system of bound atoms

The results so far where derived from considering the scattering of a neutron by a free atom. Atoms in a solid, liquid or molecular gas cannot be considered as free. They underlie interatomic forces which need to be taken into the evaluation of the cross sections.
A suitable approximation for calculating the transition operator in this case got introduced by Fermi (1936) and was later called *impulse approximation*. In this approximation the interatomic forces are neglected at the instant of collision and the transition operator is given by the *Fermi pseudopotential*

$$T \;=\; \frac{2\pi\hbar^2}{m_0}\; a\; \delta(\vec{r}). \tag{34}$$

Alternatively, with the bound scattering length b from (26)

$$T \;=\; \frac{2\pi\hbar^2}{m}\; b\; \delta(\vec{r}). \tag{35}$$

The interatomic forces are just neglected in T but not in the energy eigenstates $|\alpha\rangle$ and eigenvalues E_α.
Considering the scattering of a thermal neutron by an atom that is bound by an interatomic potential, the *differential cross section* becomes

$$\frac{\mathrm{d}\sigma}{\mathrm{d}\Omega} \;=\; |\,\langle\vec{k'}0|\,F\,|\vec{k}0\rangle\,|^2. \tag{36}$$

This describes the situation where the atom was initially in the ground state $|0\rangle$ and the neutrons energy is less than the energy separation of the ground and first excited states, which is valid for thermal neutrons. Calculating the T-matrix element in the laboratory system, with $T = \frac{2\pi\hbar^2}{m} b\delta(\vec{r}-\vec{R})$ in the impulse approximation and $\vec{q} = \vec{k} - \vec{k'}$ leads to

$$\frac{\mathrm{d}\sigma}{\mathrm{d}\Omega} \;=\; |b|^2 |g(\vec{q})|^2 \tag{37}$$

with the *ground state form factor*

$$g(\vec{q}) \;=\; \langle 0|\exp(i\vec{q}\vec{R})\,|0\rangle\,. \tag{38}$$

After Fermi (1936), see [10], an atom is said to be *strongly bound* if the relation

$$7\mathrm{fm} \;\ll\; R_0 \;\ll\; q^{-1} \tag{39}$$

with the so called *radius of the bound state* and $g(R_0^{-1}) = \frac{1}{2}$, is valid. This condition ensures that $g(q) = 1$ for the q values of interest and the scattering cross section becomes

$$\boxed{\sigma_s(\text{bound}) \;=\; 4\pi|b|^2 \;=\; \left(\frac{A+1}{A}\right)^2 \sigma_s(\text{free})} \tag{40}$$

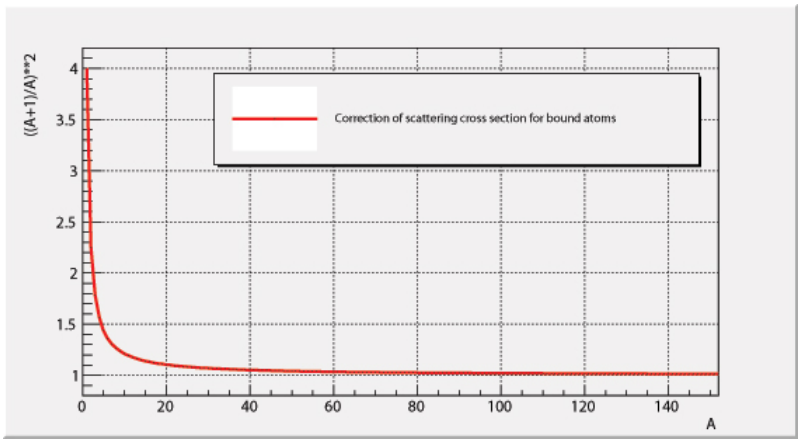


Figure 7: $\frac{\sigma_s(\text{bound})}{\sigma_s(\text{free})}$ versus mass number A.

Various experimental data confirm this result [8]. In Fig. 7 the relation is illustrated for mass numbers A up to 150.
When calculating the absorption cross section for bound atoms one finds that

$$\boxed{\sigma_a(\text{bound}) \;=\; \frac{4\pi}{k}\; b'' \;=\; \sigma_a(\text{free})} \tag{41}$$

This relation is true quite generally for any chemically bound atom and any free atom. The chemical bond in a molecule or crystal has therefore no effect on the absorption cross section. This is quite understandable as the surrounding of the atom should have no influence on whether the nucleus absorbs a neutron or not.

3.2.3 Spin dependency

So far the spin of the neutron $\vec{s}$ and the nuclear spin $\vec{I}$ have been ignored. The nuclear forces are in general spin dependent so that if $I \neq 0$ the optical potential $V(\vec{r})$ and therefore the bound scattering length b will be spin dependent.
If the neutron beam and the target are unpolarized an average over the neutron and nuclear spin states has to be made. The bound total scattering cross section σ_s is the sum of a coherent σ_c and an incoherent σ_i term

$$\sigma_s \;=\; \sigma_c \;+\; \sigma_i \;=\; 4\pi\;(|b_c|^2 + |b_i|^2) \tag{42}$$

where

$$b_c = g_+ b_+ + g_- b_- \tag{43}$$
$$b_i = (g_+ g_-)^{1/2}(b_+ - b_-). \tag{44}$$

The statistical weight factors $g_\pm$ are dependent on the nuclear spin I

$$g_+ = \tfrac{I+1}{2I+1} \tag{45}$$
$$g_- = \tfrac{I}{2I+1} \tag{46}$$

and satisfy the normalization property $g_+ + g_- = 1$. The scattering lengths $b_\pm$ in Eqs. (43)-(44) describe the situation where the spins of neutron and nucleus are parallel (b_+) or antiparallel (b_-).
The absorption cross section is dependent on the spins as well,

$$\begin{aligned} \sigma_a &= \frac{4\pi}{k} b_c'' \\ &= \frac{4\pi}{k}(g_+ b_+'' + g_- b_-'') \\ &= g_+ \sigma_{a+} + g_- \sigma_{a-}. \end{aligned} \tag{47}$$

4 Neutron fluence

4.1 Theory

In neutron capture cross section measurements one of the essential quantities is the intensity of the incident neutron beam. There are two different quantities that can be determined:

- The neutron *flux* is the number of neutrons passing through a unit area over a span of time. The unit commonly used for the flux is [neutrons/(cm^2 s)].
- The neutron *fluence* Φ is the flux integrated over a certain time period and has the unit [neutrons/cm^2].

At a TOF experiment the quantity measured is the available number of neutrons with a certain energy E_n which is the intensity of the neutron fluence and could also be denoted as the neutron flux. Crucial for all capture measurements, which are normalized to a saturated resonance at a given energy, is the shape of the fluence. This is the graph of the neutron flux over the whole energy range of the facility.
The data acquisition system (DAQ) collects the signal of the detector with a given frequency. When analysing the data, the measuring points get collected in time windows, which is equivalent to an integration over this time window given by the histogram's binning used in the analysis. The normalization has to be done over the width of the bins in order to get a figure independent of the histogram windows. If the energy, calculated from the TOF, is given in logarithmic scale, the normalization factor becomes $1/(\ln(E_{hi})-\ln(E_{low}))$, which gives the *neutron fluence in isolethargic units*.
Having a spallation target as neutron source it is common to normalize the fluence to the number of incident protons. At n_TOF the data gets normalized to $7 \cdot 10^{12}$ protons, which corresponds to a dedicated proton bunch to the facility.
It depends on the detector type if the neutrons can be measured per unit area, which would give the neutron beam profile. If not, which is the case for the fission chamber described in this thesis, the incident neutrons are measured per active area of the detector. The fluence does not get normalised to a unit area as it could well be that the beam is smaller than the active area within the fission chamber. It is important that the neutron beam thoroughly hits the active area of the device in use in order to measure the entire number of neutrons available.

When $C(E_n)$ is the total count rate coming from the detector and $B(E_n)$ the background count rate, $\Phi(E_n)$ is defined through the following relation:

$$\Phi(E_n) \;=\; \frac{(C(E_n) - B(E_n))}{\varepsilon(E_n) Y(E_n)}. \tag{48}$$

$\varepsilon(E_n)$ is the neutron detection efficiency of the apparatus and is generally also a function of the neutron energy. The reaction yield Y is the fraction of neutrons undergoing the reaction used to detect the neutrons. It can be indicated as the efficiency of the measurement.

$$\begin{aligned} Y(E_n) \quad &= \quad \frac{\text{arriving n} - \text{transmitted n}}{\text{arriving n}} \\ &= \quad \frac{\text{total number of reactions}}{\text{total number of incident neutrons}} \end{aligned} \tag{49}$$

The function of yield versus energy of the incident particles $Y(E_n)$ is referred to as yield curve or excitation function [2].
Various types of nuclear reactions, which are all energy dependent, can be used to detect neutrons. In the present fission chamber, the reaction of interest is ^{235}U(n,f). Therefore, if Φ_0 is the incident neutron fluence, the transmitted neutrons after (13) are $\Phi_0 \cdot \mathrm{e}^{-n\sigma_{fis}}$ where n is the total number of ^{235}U atoms per barn. The reaction yield is given by

$$Y(E_n) \;=\; (1 - e^{-n\sigma_{fis}(E_n)}) \tag{50}$$

and is dependent on the fission cross section $\sigma_{fis}(E_n)$ of ^{235}U and it's impurities.
If the required quantities in Eq. (48) for the detector in use are known, the neutron fluence can be measured.
The methods for determining $\Phi(E_n)$ used at the commissioning of the new spallation target at n_TOF in summer 2009 are listed and briefly described in the next section.

4.2 Fluence measurements at the n_TOF commissioning 2009

During the commissioning phase 2009 at n_TOF the neutron fluence was measured in different ways:

- PTB fission chamber: ^{235}U
  Nuclear reaction: ^{235}U(n,f)
  The cross section of ^{235}U is a standard at thermal energies [11] and above the resonance region [12] (0.1 - 20 MeV). The intensity and the shape of the fluence was determined in these energy regions.
- Silicon detectors: ^{6}Li
  Nuclear reaction: ^{6}Li(n,t)^{4}He
  The cross section of this reaction is a standard from thermal energies up to 100 keV [13].
- Monitoring micromegas detector: ^{10}B and ^{235}U
  Nuclear reactions: ^{10}B(n,α)^{7}Li and ^{235}U(n,f)
  The cross section of ^{10}B(n,α)^{7}Li is a standard from thermal energies up to 200 keV [14].
- C6D6 detectors: double foil method
  Nuclear reaction: ^{197}Au(n,γ) - ^{198}Au(β)
  The intensity of the flux at 4.9 eV was determined.
- TAC detector: saturated resonances method
  Nuclear reaction: ^{197}Au(n,γ)
  The intensity of the flux at 4.9 eV was determined.

4.2.1 Flux measurement using the Micromegas detector

A new in-beam neutron flux detector, based on the Micromegas technology, has been developed for n_TOF [15]. The principle is based on the detection of electrons created by ionization of the filling gas by charged particles.
The gas volume is separated in two areas by a very thin micromesh. In the first region the conversion and drift of the ionization electrons takes place. The second volume, 50-160 micrometer thick, is for the signal amplification. The association of the micromesh and the anode pad is called Micro-Bulk. A high field (40 to 70 kV/cm) is created by applying a few hundred volts. The anode pad, which can be segmented into strips or pads, collects the charge produced by the avalanche process. The positive ions drift to the micromesh.

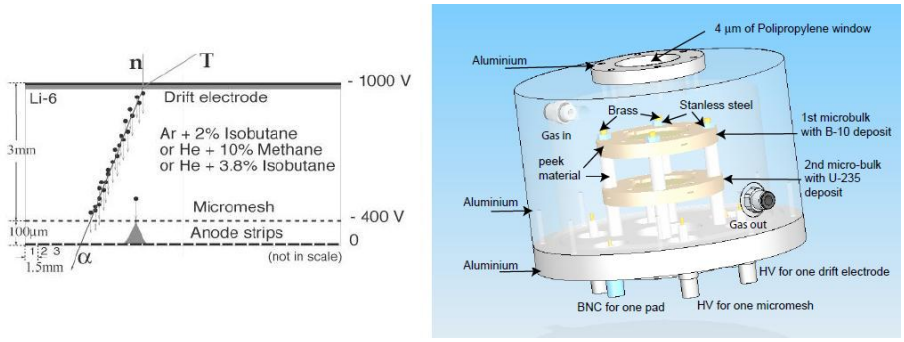


Figure 8: Developed Micromegas detector; working principle, after [16], on the left and design, after [15], on the right.

The developed neutron beam monitor, see Fig. 8, contains two separate microbulks with differing neutron/charged particle converters.

- The first drift cathode is made of 12 μm coppered Kapton with about 1 μm of ^{10}B. The α particles and the ^{7}Li ions emerging from the reaction ^{10}B(n,α)^{7}Li can be distinguished through the different amplitude they produce in the detector.
- The second drift cathode is made of 1.5 μm aluminised Mylar with 1 mg of ^{235}U (99.94%). The fission products can again be differentiated from the α background, coming from the natural decay of ^{235}U, through the differing energy deposition within the detector.

The usage of two different converter materials has a great advantage for the flux measurement. The fluence over a wide range, namely from thermal up to a few MeV, can be measured with this detector. As ^{235}U has a pronounced resonance structure it can be successfully used only at low energies and above a few 100 eV. For the energy region in between ^{10}B is a well suited standard.
There is still an uncertainty about the exact mass of the ^{10}B deposit in the detector. The alignment of the detector has to be made rather carefully, as the active area of this deposit is about the same size as the neutron beam. There were certain difficulties at the commissioning to assure the necessary accuracy of the alignment.
Furthermore the diameter of the ^{235}U deposit is smaller than the diameter of the beam.
Due to the latter reasons the data taken with the Micromegas detector was treated carefully by the n_TOF collaboration.

4.2.2 Flux measurement using the silicon monitor

The installed silicon monitor at n_TOF is an on-line neutron flux detector [17]. It contains a 1.5 μm thick Mylar foil with a ^{6}LiF deposit of 500 μg/cm^2, placed orthogonal to the neutron beam. Four silicon detectors are mounted symmetrically around and outside the beam to measure the emitted α particles and tritons from the deposit after interaction with an incoming neutron. A schematic view of this flux monitor can be seen in Fig. 9

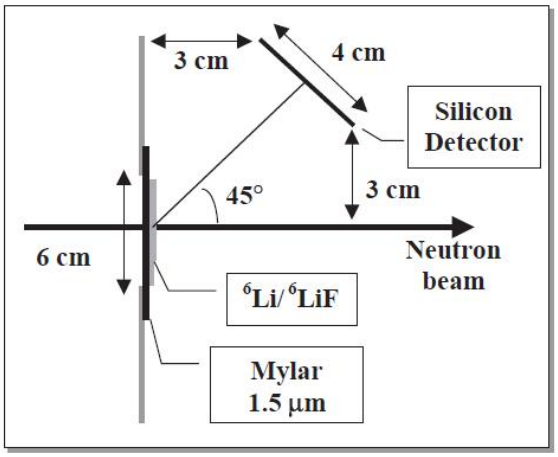


Figure 9: Schematic view of the silicon monitor, after [17].

The detected particles can be distinguished through the energy deposited in the Si of the detector. The α particles exhibit a wide energy spectrum and fall sometimes below the threshold of the Flash analog to digital converters (ADC). Therefore just the signals from the tritons coming from the ^{6}Li(n,α)t reaction are taken into account for the evaluation of the neutron fluence.

When $\mathrm{d}N_{Si}/\mathrm{d}\ln E$ represents the distribution of detected events in the Si monitor, which is normalized to 7x10^{12} protons, the isolethargic neutron intensity can be extracted from the data through the following expression:

$$\frac{\mathrm{d}n}{\mathrm{d}\ln E} = \frac{\mathrm{d}N_{Si}}{\mathrm{d}\ln E} \cdot \frac{1}{Y \cdot \varepsilon}.$$

Y is the capture yield for ^{6}Li and ε is the geometric efficiency. Due to the design of the detector, the geometric efficiency is a complicated function of the neutron energy and has to be determined performing a Monte Carlo simulation under consideration of the exact geometry of the apparatus.

The neutron flux determination with the Si monitor underlies systematic uncertainties associated with the simulation of the geometric efficiency, the uniformity and thickness of

the ^{6}LiF deposit and the evaluation of the total proton number in the measurement. A combination of all these effects can lead to an uncertainty of 10-20 %.

4.2.3 The double foil method

In the double foil method two foils of the same material, that has one large and isolated resonance, are activated. The two foils are overlapping and get activated under the same neutron beam. The thickness of the foils is chosen in such a way that the foil that is hit by the beam first entirely depletes the flux at the considered resonance energy. The rest of the spectrum is left almost unchanged.
The neutron flux can be determined by considering that the relation between the resonance energy E_{res} of the neutrons and the flux around the resonance is:

$$\mathrm{d}\Phi \;=\; \frac{C}{\mathrm{d}E_{res}}. \tag{51}$$

In the ideal case, where there is a negligible contribution from the domain outside the resonance energy, the neutron flux at E_{res} will be calculated using

$$N_{F_1} - N_{F_2} \;=\; C\ (2I(d) - I(2d)), \tag{52}$$

where N_{F_i}, $i = 1, 2$, is the number of nuclei of a certain isotope created in the foil i through neutron capture and d is the thickness of the foils. Substituting C in Eq. (51) leads to the relation

$$\Phi \;=\; \frac{N_{F_1} - N_{F_2}}{(2I(d) - I(2d))} \cdot \frac{1}{E_{res}}. \tag{53}$$

A typical example for a material with such a large isolated resonance at 4.9 eV is Au. ^{197}Au creates through neutron capture the isotope ^{198}Au. With a half-life of 2.69 days ^{198}Au β decays to ^{198}Hg*, which de-excites in 99 % by emitting a 411.8 keV γ-ray.

$$^{197}Au(n,\gamma)^{198}Au \;\overset{\beta^-}{\rightarrow}\; ^{198}Hg \tag{54}$$

As the cross section of Au is also high at thermal energies, the Au foils get wrapped in a Cd shielding to prevent capture of thermal neutrons. By measuring the number of 411.8 keV photons, which are proportional to the number of ^{198}Au nuclei, during an acquisition time at the end of the activation, the flux at the resonance energy can be calculated [18].

4.2.4 The saturated resonance method

The capture yield $Y(E)$, i.e. the fraction of incident neutrons undergoing a (n,γ) reaction, gets determined in a neutron capture experiment. With $0 < Y(E) < 1$ and the thickness n of the analysed material, i.e. number of atoms per barn, the yield can be written as

$$Y(E) \;=\; (1 - e^{-n\sigma_{tot}(E)}) \cdot \frac{\sigma_\gamma(E)}{\sigma_{tot}(E)} \;\approx\; \begin{cases} n \cdot \sigma_\gamma & \text{if } n \cdot \sigma_{tot} \ll 1 \\ \frac{\sigma_\gamma}{\sigma_{tot}} < 1 & \text{if } n \cdot \sigma_{tot} \gg 1, \end{cases} \tag{55}$$

where the approximations for thin respectively thick samples is given [6].
So called "saturated" resonances can be used to determine either the neutron fluence or the efficiency of a detector [19]. This refers to resonances where the thick sample approximation is valid in the peak of the resonance. The capture yield therefore becomes proportional to the ratio of the capture and the total cross section.

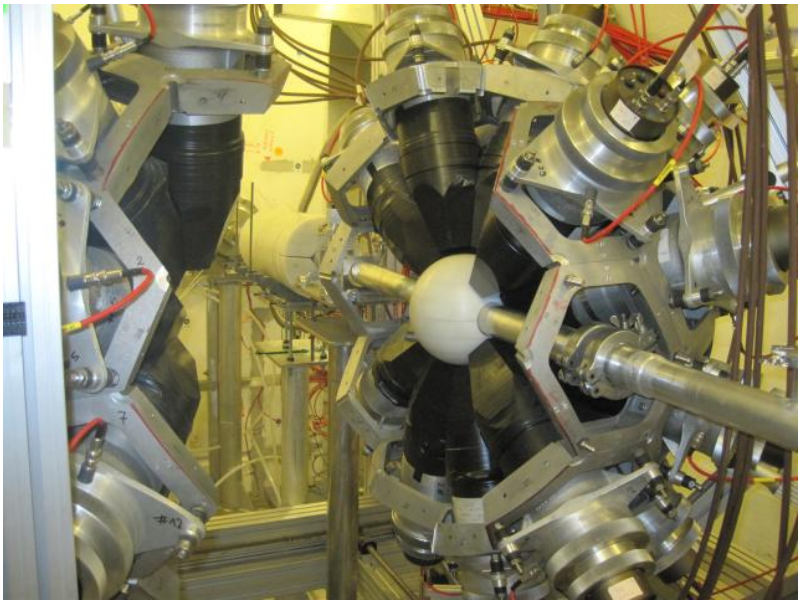


Figure 10: Opened 4π Total Absorption Calorimeter; in the middle the spherical neutron absorber/moderator for reducing the background from scattered neutrons can be seen.

At the commissioning, the saturated resonance method has been used to determine the flux at 4.9 eV by measuring a Au ring, to test the alignment of the experiment, and a 4 cm diameter Au sample of 25 mm thickness, with the Total Absorption Calorimeter (TAC), see Fig. 10. This γ-ray detector satisfies the properties of a large solid angle coverage, high total γ-ray efficiency, good energy resolution, high segmentation, low neutron sensitivity and fast time response [19].

In order to measure the neutron fluence Eq. (48) is used. The γ-ray efficiency of the TAC has been determined by Monte-Carlo simulations.

5 Fission chamber

The fission chamber used at the commissioning of the new n_TOF target in summer 2009 is a property of the Physikalisch Technische Bundesanstalt (PTB) Braunschweig. In the following it is sometimes called PTB chamber.

5.1 Chamber design

The electrode assembly contains five Pt backed fission foils which contain ^{235}U deposits and six Ta collector plates. Each of these eleven circular plates has a diameter of 86 mm and is 0.125 mm in thickness. Separated through spacers, the interelectrode gap is 5 mm. The assembly is held together by six small diameter nylon rods. Light struts attach the formation to the cylindrical chamber body, which is pressed from 0.55 mm thick stainless steel. The overall length of the fission chamber along its axis, which is parallel to the direction of the incident beam, is 50 mm and the chamber is closed by two 0.15 mm thick Ta windows.
The need of fast timing resolution as well as the need for good discrimination between pulses from fission fragments and alpha particles demands a compromise which results in the chamber dimensions [20].
The materials in use were chosen as they do not have, as Al for example, a pronounced structure in their neutron scattering cross sections at lower energies. Additionally Pt is a stable backing material for the fissile deposit, as it is reasonably chemically inert in air at normal temperatures.

5.2 Mode of operation

In operation a continuous gas flow through the chamber at atmospheric pressure was provided. The gas was a mixture of 90% Argon and 10% CF_4.
Under irradiation with a neutron beam the fission fragments, coming from the ^{235}U deposit, ionize the gas. By applying a voltage on the electrodes the charge, proportional to the ionization energy of the particles, gets measured.
As ^{235}U is a natural radioactive material, it is important to distinguish the signals coming from the α particles, caused by the natural decay of the material, from the fission fragments. These considerations have been taken into account in the design of the chamber and explain the very thin ^{235}U deposits on the electrodes [20].

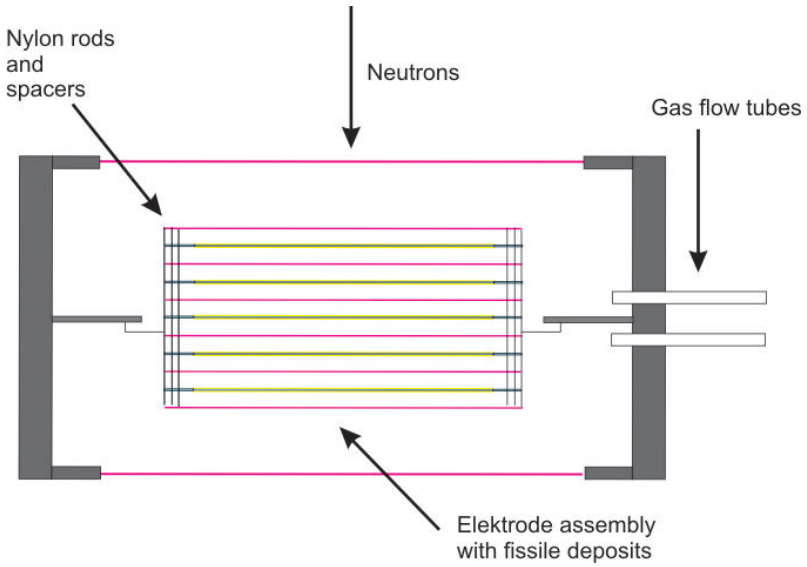


Figure 11: Schematic drawing of the fission chamber, the ^{235}U deposits are drawn in yellow.

5.3 ^{235}U chamber data

The fissile material of the chamber, ^{235}U, has been painted on each side of the Pt plates. Approximately 5 μg/mm^2 over a circular area of 76 mm diameter has been deposited in multiple coats. The stated thickness is approximate and does not differ in any one area of 100 mm^2 by more than 6% from the average of the foil. The total deposit mass is on all 10 sides of the Pt foils within 2.2% of the average.
The total mass of fissile deposit in the chamber is [20]:

$$\begin{aligned} 201.4 \pm 0.5 \text{ mg} \quad & \text{by weighing} \\ 202.7 \pm 1.4 \text{ mg} \quad & \text{by alpha counting.} \end{aligned}$$

The contents of the fissile deposit are:

Isotope	Abundance (atom%)
^{235}U	99.9183 $\pm$ 0.0003
^{234}U	0.0362 $\pm$ 0.0002
^{236}U	0.0094 $\pm$ 0.0001
^{238}U	0.0361 $\pm$ 0.0002

5.3.1 Nuclear reactions and fission products

The probability for spontaneous fission of ^{235}U is so small ($7.0 \cdot 10^{-9}$ %) that it decays, with a half-life of $703.8 \cdot 10^6$ years [21], completely through emission of an α particle.

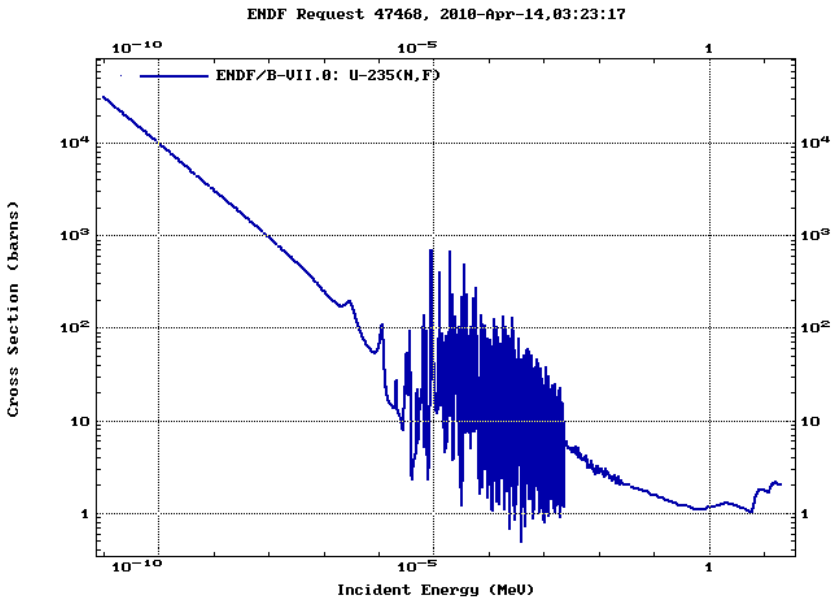


Figure 12: Fission cross section of ^{235}U, after [1].

^{235}U has a very high fission cross section at thermal energies, see Fig. 12. The output of the reaction

$$^{235}U \; + \; n \; = \; ^{236}U \tag{56}$$

leads to a nucleus with both an even number of protons and neutrons. The binding energy of a nucleus increases in this case. It can be understood via the pairing energy term in the semi-empirical mass formula from C.F.Weizsäcker.

$$E_B \; = \; a_V \; A \; - \; a_S \; A^{2/3} \; - \; a_C \frac{Z^2}{A^{1/3}} \; - \; a_A \frac{(N-Z)^2}{A} \; + \; \Delta \tag{57}$$

As Eq. (57) shows, the binding energy E_B of nucleons consists of a volume term, a term for surface effects, a coulomb term, a term that accounts for the differences of proton and neutron numbers (asymmetry term), and of the pairing energy term Δ,

$$\Delta \; = \; \frac{a_P}{A^{1/2}} \delta \tag{58}$$

with

$$\delta = \begin{cases} 1, & \text{for ee nuclei} \\ 0, & \text{for eo- or oe- nuclei} \\ -1, & \text{for oo nuclei} \end{cases}, \tag{59}$$

where e stands for even and o for odd. On the first position is the number of protons and on the second the number of neutrons.

In the case of ^{235}U, if a thermal neutron strikes the nucleus, the excitation energy becomes 6.4 MeV, which is 0.1 MeV higher than the fission barrier. This leads to the high cross section that can be seen in Fig. 12.

The fission products show an asymmetric mass distribution as shown in Fig. 13. This comes from the shell structure of nuclei. Nuclei with the magic neutron number 82 are much more stable than others.

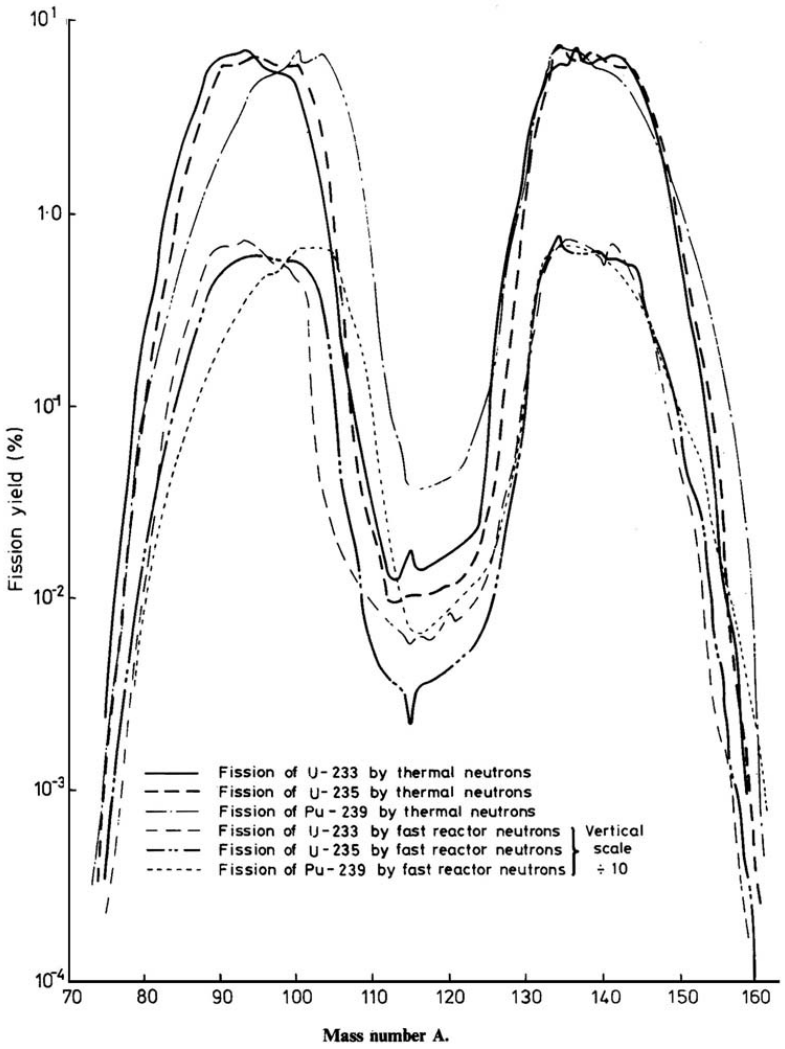


Figure 13: Fission product yield of different materials, after [22].

5.4 Experimental setup

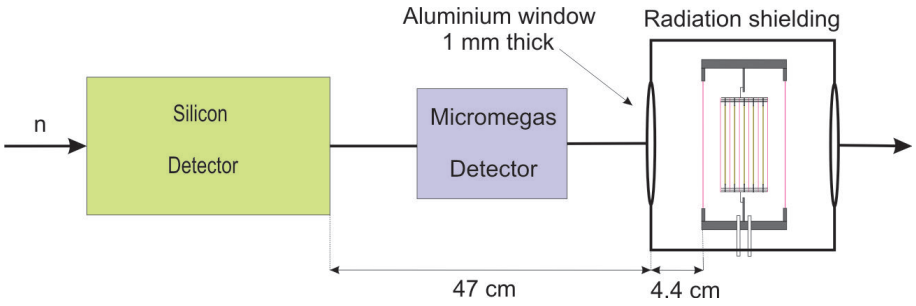


Figure 14: Original experimental setup with the PTB chamber. The Micromegas detector was removed, leaving 47 cm of air between the silicon detector and the radiation shielding of the PTB chamber.

In Fig. 14 the setup for the neutron fluence measurement with the PTB chamber is drawn. The silicon detector (SILI) is the first detector in the experimental area and is fixed to the entrance wall.

Originally the Micromegas detector (MGAS) was placed behind the SILI. Due to alignment problems it had to be removed as the counting rate in the PTB chamber was decreasing significantly. See Sec. 6 for details.

The PTB chamber was mounted inside a radiation shielding container made of Al. Inside this container it was positioned 4.4 cm behind the Al entrance window of the container.

The fission chamber was operated with 250 V static voltage. The signal of the fission chamber was split into 3 data acquisition (DAQ) channels with varying parameters, as listed in Table 1. Each of the channels was operating with 100 Megasamples per second (MS/s).

The first channel had a dynamic range of 1V in order to easily distinguish between the α

Identifier	Dynamic Range [V]	Delay [μs]
Det. 1	1	5
Det. 2	2	8000
Det. 3	2	5

Table 1: Configuration of the three data acquisition channels of the fission chamber.

particles from the natural decay of Uranium and the fission fragments. Channel 2 and 3 had a dynamic range of 2 V to minimize the saturation.

The second channel was meant to be set up with an 8 ms delay in order to also measure the signals of thermal neutrons. Due to a misconfiguration of the DAQ system the data recorded by this channel cannot be taken into account for the evaluation of the neutron fluence.

5.4.1 Materials in the experimental setup

When calculating the neutron flux in the experimental area from the recorded data, some corrections have to be made for the materials present in the neutrons flight path and inside the fission chamber. In Table 2 the materials that need to be accounted for are listed.

Material	Length	Position
in flight path:		
Air	470 mm	between SILI and PTB
Al and impurities	1 mm	entrance window of radiation shielding
Air	44 mm	between Al-window and PTB
inside fission chamber:		
Ta	0.775 mm	entrance window and electrode material
Pt	0.625 mm	electrode material
U isotopes		^{235}U deposit and impurities

Table 2: Materials in the neutron flight path in the experimental area, before and within the PTB fission chamber. The calculated neutron flux needs to be corrected for the losses of neutrons through the interactions with these materials.

6 Data analysis

6.1 Experimental data

During the commissioning phase in summer 2009 at n_TOF a total of 151 experimental runs (run nr. 9210 - 9370) with the PTB chamber were recorded. This includes all the measurements of the setup phase of the fission chamber, the background measurements and other experimental runs without protons for adjustments in the experimental area.

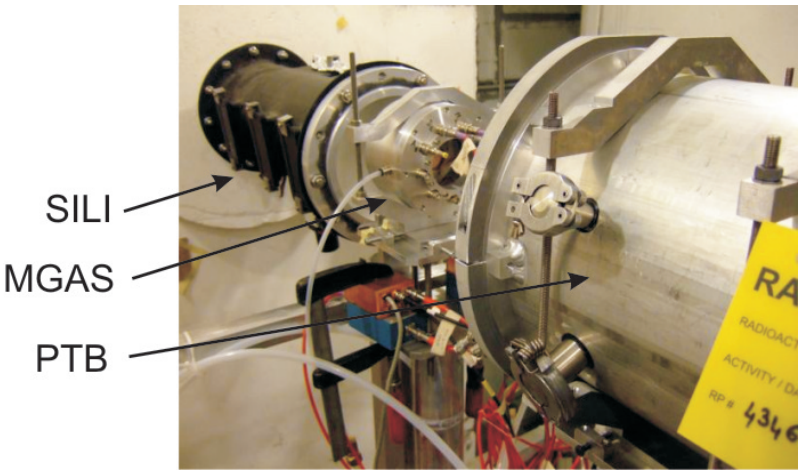


Figure 15: Original setup with silicon monitor, Micromegas detector and PTB chamber, inside the radiation protection container, behind each other at the commissioning.

There are a few experimental runs, listed in Table 3, which cannot be taken into the data analysis for the neutron fluence.

The original setup with the Micromegas detector in front of the PTB chamber, see Fig. 15,

Run Numbers	Reason for dismissing the data
9210 - 9224	Configuration of the DAQ
9225 - 9230	MGAS shielding the fission chamber
9256 - 9257	Sweeping magnet off
9295 - 9305	MGAS shielding the fission chamber

Table 3: Experimental runs that are not taken into account in the data analysis for the quoted reasons.

had to be altered due to alignment problems. The shielding effect of the MGAS detector can easily be seen in Fig. 16. Especially in the low energy region, respectively high time of flight region, the decrease in the counting rate is up to 20%. The Micromegas detector

has been removed, leaving 47 cm of air between the silicon detector and the fission chamber.

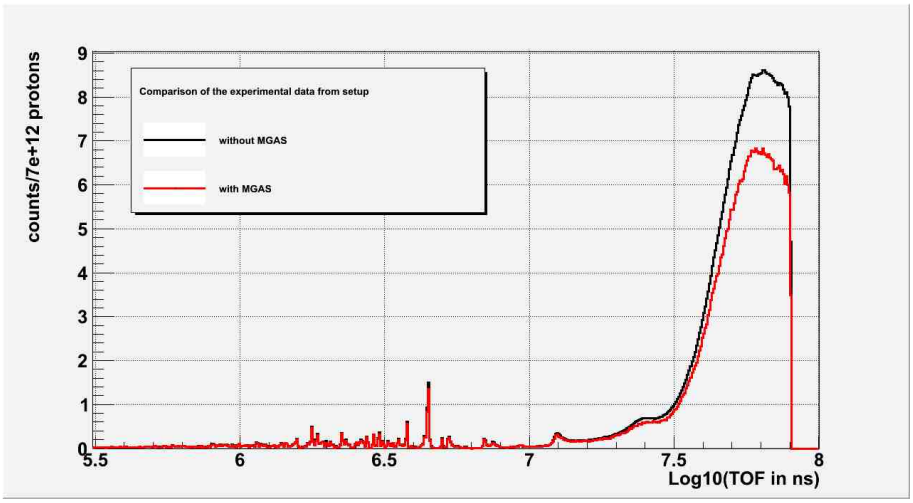


Figure 16: Comparison of the time of flight spectra from runs with and without the MGAS detector in front of the fission chamber.

Ninety experimental runs were taken into the evaluation of the neutron fluence with the PTB chamber. The total number of protons delivered from the PS for these experimental runs was $8.87 \cdot 10^{17}$ protons as dedicated and parasitic pulses.

At n_TOF the neutron flux data get's normalized to an average proton pulse coming



Figure 17: Experimental data

from the PS of $7 \cdot 10^{12}$ protons per pulse [ppp]. In Fig. 17 the experimental data collected with the PTB chamber is plotted against the neutron energy.

In Fig. 18 the relative error of the experimental data is plotted. The error in the low energy region is, due to the high counting rate, less than 1 %. This is the desired accuracy [5].

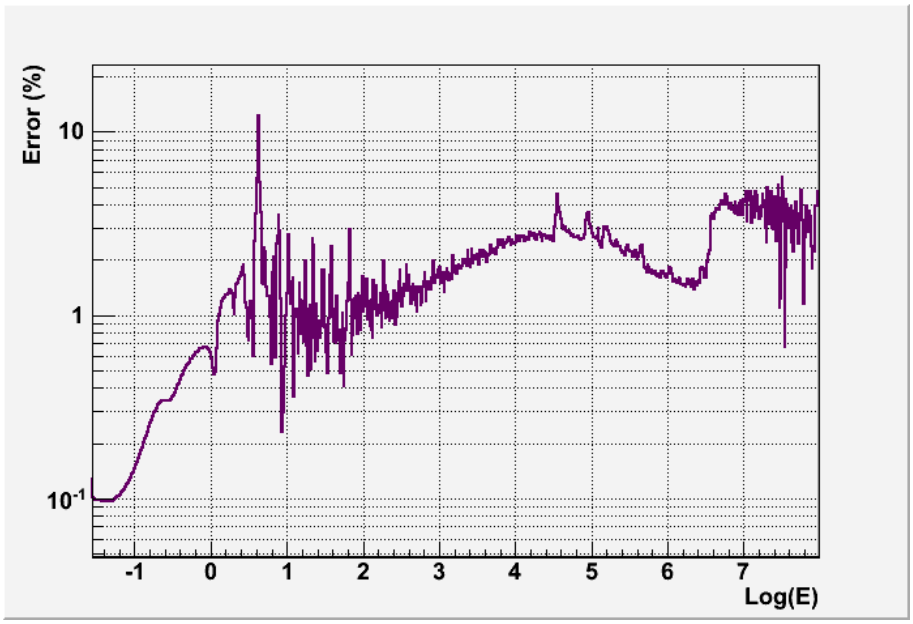


Figure 18: Relative error of the experimental data in %.

6.2 Background

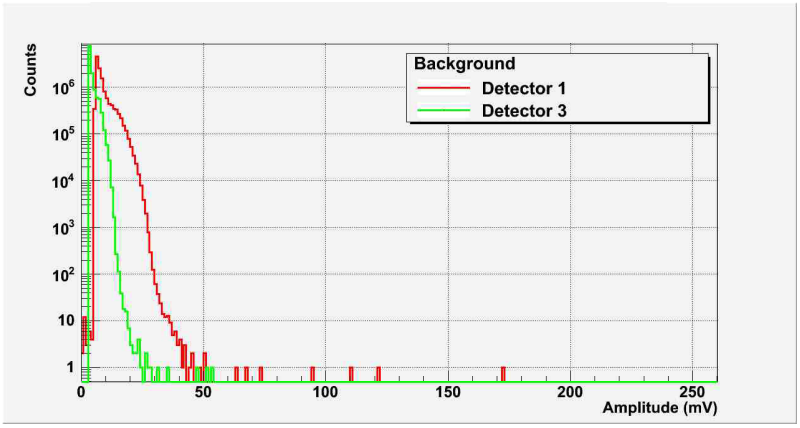


Figure 19: Background measurement of the PTB chamber.

In order to determine the α particle background, resulting from the natural decay of ^{235}U, a background measurement has been performed on the 3rd of August 2009. The background has been measured for 3 h, 28 min and 26 s. The result can be seen in Fig. 19.
In Fig. 20 and Fig. 21 the background is compared with the results of one experimental

run in order to determine the background correction for the experimental data. The fission products of neutron induced fission have a higher energy than the alpha particles, resulting in a higher amplitude in the experimental data. Therefore a threshold point for the two detector exits used in the analysis can be determined.
The background counts of the experimental data with higher amplitudes than the threshold amplitude A_{th} are less then 1 %. Therefore only data points with an amplitude bigger than A_{th}, as listed below, have been used in the evaluation of the neutron fluence.

Detector Exit 1:	A_{th}	=	32 mV
Detector Exit 3:	A_{th}	=	16 mV

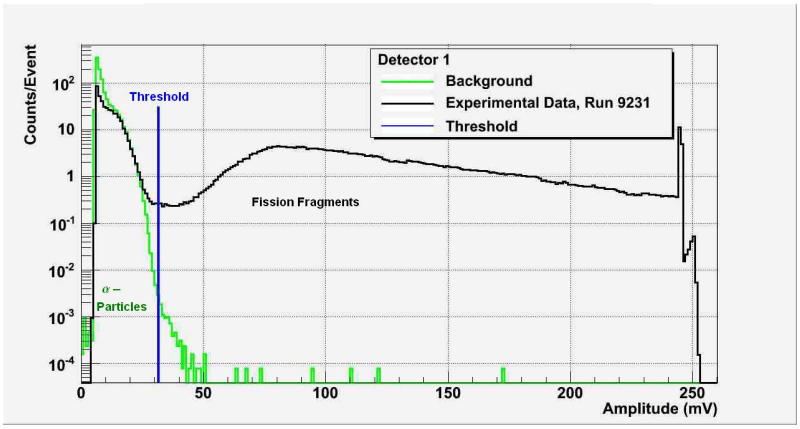


Figure 20: Pulse height distribution of the data from detector 1.

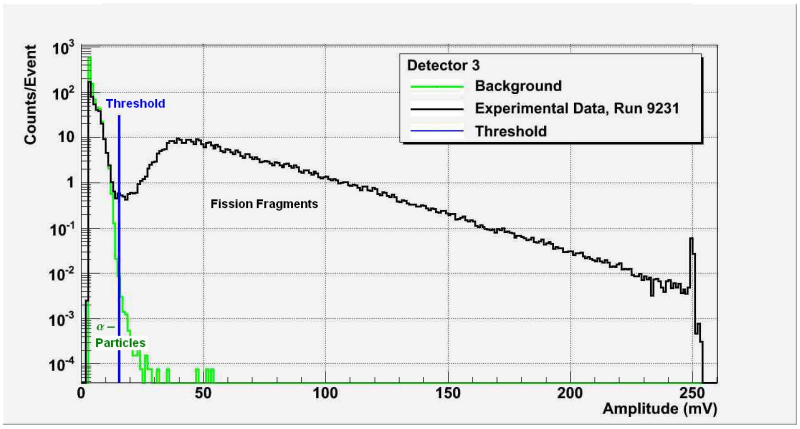


Figure 21: Pulse height distribution of the data from detector 3.

6.3 Corrections for the materials present

In order to find the correction for the neutron losses within a layer of thickness x, of any given material i, the transmission through that layer has to be calculated using the following relation

$$n(x) \;=\; n(0) \cdot \underbrace{\exp(-N_{mole}\; x \sum_{i} n_i\; \sigma_i)}_{Transmission}\,. \tag{60}$$

N_{mole} is given by Eq. (16) and represents the number of molecules per cubic centimeter. If the material is not made of molecules but is rather a mixture of different isotopes, meaning a substance with impurities of which the weight % are known, the contribution of each isotope needs to be accounted for in the density of the actual material.
n_i is the number of atoms with the cross section σ_i within the molecule, or the material.
If the total $\sigma_{(n,tot)}$ or just the absorption cross section $\sigma_{(n,\gamma)}$ is taken in the calculation depends on the geometry of the experiment and is mentioned in each of the chapters below.
The data for the cross sections of all the materials has been taken from the ENDF/B-VII.0 database.

6.3.1 Air

In the experimental setup with the fission chamber there were 47 cm of air in between the fission chamber and the silicon monitor at the entrance of the experimental area. In order to calculate the correction for the losses of neutrons in air, the total cross section $\sigma_{(n,tot)}$ of the isotopes in air have been taken into account. This means that any reaction of a neutron with a nucleus in the gas leads to the loss of the neutron.
The assumption that a scattered neutron is not going to be detected in the fission chamber is valid as the error made with this model is less than 1 %, see Sec. 9.1.2 for details.

In the calculation for the losses of neutrons in 47 cm of air the composition of air was

Molecule	% by volume	considered isotopes
N_2	77.024	100% ^{14}N
O_2	20.642	100% ^{16}O
Ar	0.924	99.6% ^{40}Ar
		+ 0.4% ^{36}Ar
H_2O	1.41	100% ^{1}H,
		100% ^{16}O

Table 4: Composition of air as assumed in the calculation.

assumed to be like listed in Table 4. Trace gases, such as CO_2, NH_3, He and others, have

not been considered in the calculation.

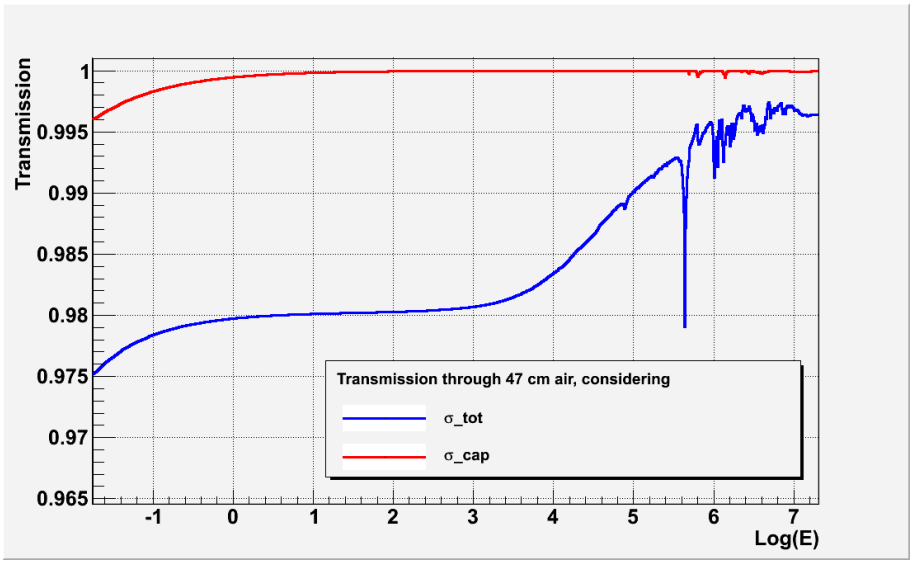


Figure 22: Correction factor for 47 cm of air, calculated with $\sigma_{(n,tot)}$ in blue and with $\sigma_{(n,\gamma)}$ in red.

For the humidity in air 50% relative atmospheric moisture was taken as the average, at an ambient temperature of 23°C in the experimental area and an atmospheric pressure of 1013.2 hPa.
In order to calculate the number of atoms per barn the density of air at 23°C, $\varrho_{air} = 1.192$ [kg/m^3], was used. The molar mass of air was taken as $M = 0.029$ [kg/mol].
The total effect of the 47 cm of air can be seen in Fig. 22. In the low energy region a maximum of 2.5% of the neutrons are lost from the beam. If the calculation is done with the capture cross section $\sigma_{(n,\gamma)}$ only, the transmission through the layer would be according to the red graph and could be neglected. This approach would not reflect the circumstances at the experiment correctly.

6.3.2 Al window

The radiation protection container of the fission chamber was made of Al. In Fig. 23 the setup at the commissioning can be seen. The neutron beam entered the Al container through the 1 mm thick entrance window.
The contents of the Al window are listed in Table 5.
In Fig. 24 the correction factor for the Al window with all the impurities, as listed in Table 5, is illustrated in blue. The pronounced resonances at 337, 1098 and 2325 eV is due to

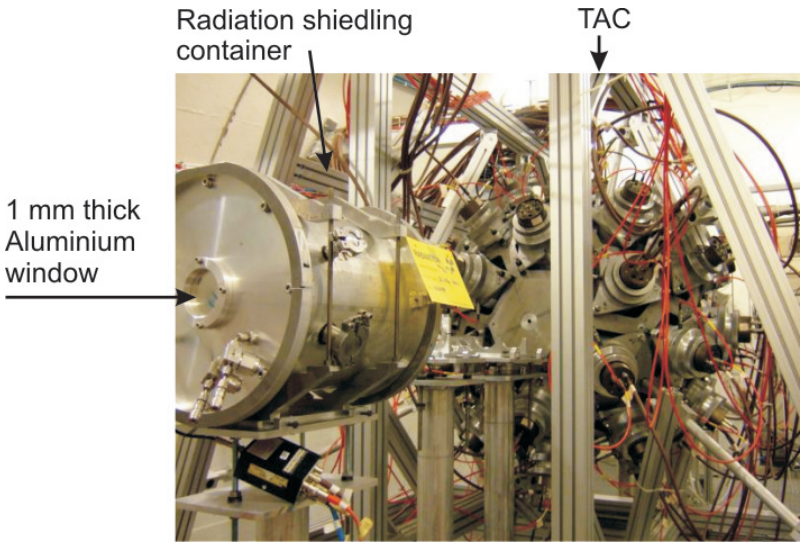


Figure 23: Radiation protection container with the PTB fission chamber and TAC in the experimental area.

Mn contained within the window. Although the proportion of Mn is as small as 0.5 weight % the effect is not to be neglected as the total cross section at these resonances is of the order 10^3 barn. Fe also has a pronounced resonance structure in the keV region with a cross-sectional value of maximal 300 barn. Due to the difference in the cross section of one order of magnitude, the influence of Fe is not visible in the correction factor.

chem. Element	Abundance (weight%)	Density ϱ [g/cm^3]	Molar Mass M [g/mole]
Al	94.95	2.70	26.982
Mg	3	1.738	24.305
Mn	0.5	7.21	54.938
Si	0.4	2.329	28.086
Fe	0.4	7.874	55.845
Cr	0.3	7.19	51.996
Zn	0.2	7.14	65.38
Ti	0.15	4.506	47.867
Cu	0.1	8.94	63.546

Table 5: Contents of the Al window of the radiation shielding container.

In the low energy region the difference between the calculation of the correction factor considering pure ^{27}Al and all the materials present in the window is less than 0.2%. As the cross section of ^{235}U is not an energy standard in the resonance region, the effect of Mn and all the other impurities can be neglected.
The total cross section $\sigma_{(n,tot)}$ has been taken for evaluating the transmission through the window. The error made through assuming scattered neutrons as beeing lost is less than

0.1 %, see Sec. 9.1.2 for details.
When considering the correction of the scattering cross section for the strong chemical bonding of the atoms in the window, one finds that the initial raise of the cross-sectional value by about 7% just leaves 0.07% difference in the correction factor, which is due to the exponential function in Eq. (60).

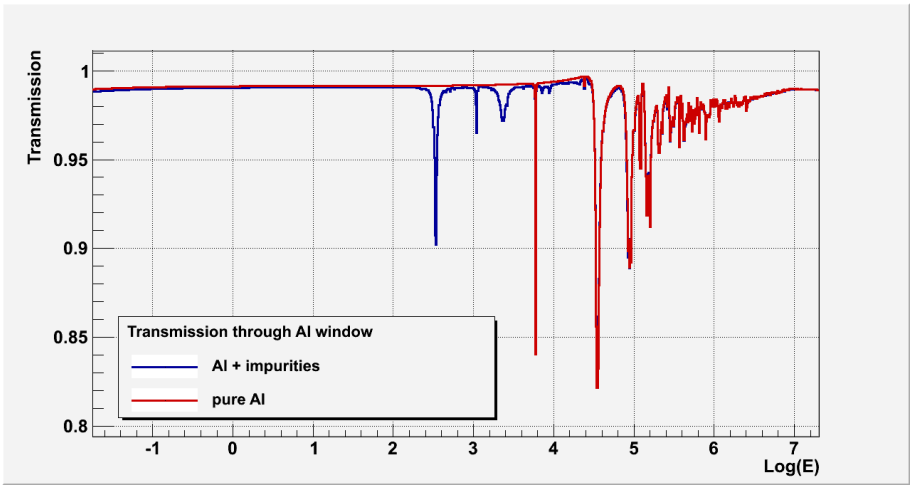


Figure 24: Correction factor for the Al window in blue. In comparison the correction for pure ^{27}Al is shown in red.

In total the approximations made by taking $\sigma_{(n,tot)}$ of pure ^{27}Al makes an error of less than 0.37%.

6.3.3 Air within the radiation shielding

Between the Al window of the radiation shielding and the fission chamber were 4.4 cm of air. The neutron losses in such a small air layer is less than 0.24 % if assumed that the scattered neutrons also get lost from the beam. If just the absorbtion of neutrons in air is taken into account, which would be the more realistic approach due to the proximity of this air layer to the fission chamber, an effect of 0.04% at the maximum is obtained.
The experimental data has not been corrected for the rather small losses of neutrons in this layer.

6.3.4 Ta window

At the entrance to the fission chamber there is a window made of $d = 0.15$ mm thick Ta. The correction for the losses in this window are shown in Fig. 25.
As the window is very close to the inside of the fission chamber, only capture events are to be taken into account for the neutron losses.

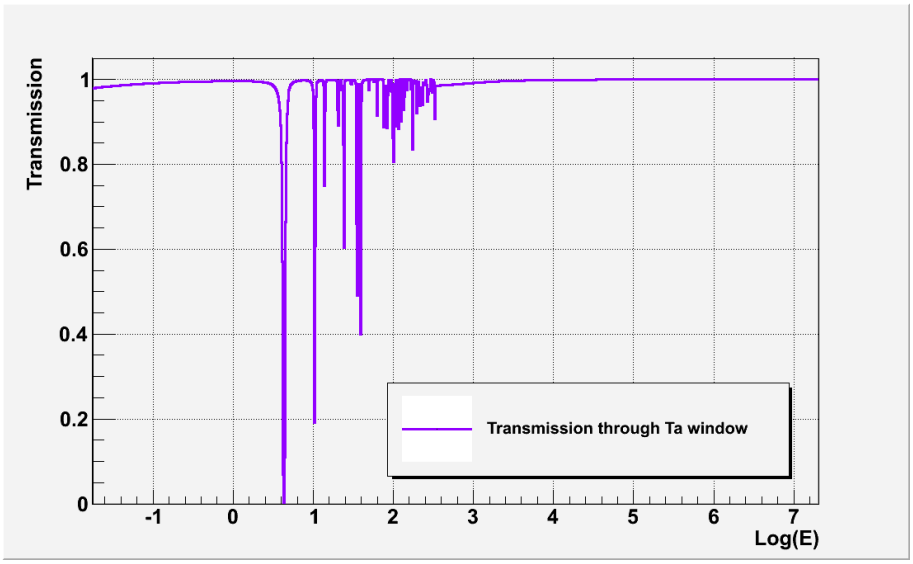


Figure 25: Correction for the Ta window.

6.3.5 Multilayer structure of the fission chamber

The signals measured in the fission chamber are the sum of all the fission events happening at a given time. It is not possible to distinguish in which of the ^{235}U layers the fission actually occurred.
When looking at the multilayer structure of the detector, it is clear that the last ^{235}U deposit will, due to absorption events in all the previous layers of material, not get hit by as many neutrons as the first one. This is equivalent to the statement that the last ^{235}U deposit measures a diminished flux. A correction for the multilayer structure must therefore be applied to the calculated fluence.
The contribution to the detector signal coming from each of the 10 deposits c_i is proportional to the incident fluence Φ_i at this particular ^{235}U layer. The total count rate C, meaning the signal of the detector, is given by

$$C = \frac{1}{10}\sum_{i=0}^{10} c_i \propto \frac{1}{10}\sum_i \Phi_i = \Phi_0 \frac{1}{10}\sum_i \mathrm{e}^{-\sigma_i^{cap}\ n_i}. \tag{61}$$

Where n_i is the number of atoms per barn of a given material in the flight path and σ_i^{cap} is the capture cross section of this material. Φ_0 is the fluence before the fission chamber. When Φ_1 is the neutron fluence hitting the first ^{235}U deposit, Φ_0 must be corrected for the neutron losses within the first Ta electrode.

$$\Phi_1 \;=\; \Phi_0 \cdot \mathrm{e}^{-\sigma_{Ta}^{cap}\; n_{Ta}}$$

The second ^{235}U layer gets hit by the neutron fluence Φ_2 which is given by:

$$\Phi_2 \;=\; \Phi_0 \cdot \mathrm{e}^{-\sigma_{Ta}^{cap}\; n_{Ta}} \mathrm{e}^{-\sigma_{Pt}^{cap}\; n_{Pt}} \mathrm{e}^{-\sigma_{U}^{cap}\; n_{U}}.$$

In the following the corrections for the materials will be denoted as listed below:

$$\begin{aligned} T &= e^{-\sigma_{Ta}^{cap}\; n_{Ta}} \\ P &= e^{-\sigma_{Pt}^{cap}\; n_{Pt}} \\ U &= e^{-\sigma_{U}^{cap}\; n_{U}}. \end{aligned}$$

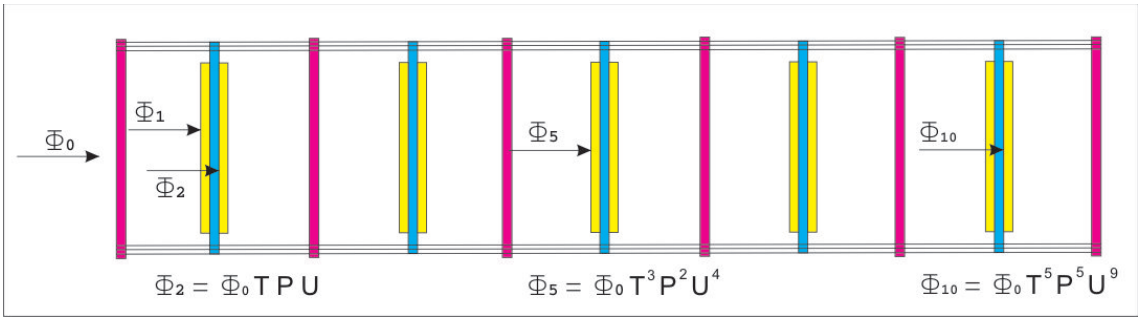


Figure 26: Schematic view of the fission chamber with all layers. Ta electrodes in magenta, Pt electrodes in blue, and U layers in yellow. The incident neutron flux is described below for the second, the fifth and the last U layer.

The corrections for the losses before each of the ^{235}U layers, which can be verified with Fig. 26, sums up to

$$\begin{aligned} C \;&\propto\; \Phi_0 \;\tfrac{1}{10}\; \sum_i \mathrm{e}^{-\sigma_i^{tot}\; n_i} \\ &=\; \Phi_0 \;\tfrac{1}{10}\; \Big[T + TPU + T^2U^2P + T^2U^3P^2 + T^3U^4P^2 + T^3U^5P^3 \\ &\qquad + T^4U^6P^3 + T^4U^7P^4 + T^5U^8P^4 + T^5U^9P^5 \Big] \\ &=\; \Phi_0 \;\tfrac{1}{10}\; \Big[\big(T + TUP\big) \cdot \big(1 + TU^2P + (TU^2P)^2 + (TU^2P)^3 + (TU^2P)^4\big) \Big]. \end{aligned} \tag{62}$$

As an approximation it can be considered that all the material present in the chamber is collected in a layer in front of the active area of the detector. The correction made in this manner will give a figure for the neutron losses that is too big. Considering only half of the actual amount of each material is a better approach.

$$C \propto \Phi_0 \cdot \mathrm{e}^{-\sigma_{Ta}^{cap} \frac{n_{Ta}}{2}} \mathrm{e}^{-\sigma_{Pt}^{cap} \frac{n_{Pt}}{2}} \mathrm{e}^{-\sigma_{U}^{cap} \frac{n_{U}}{2}} \tag{63}$$

The effect of these corrections is drawn in Fig. 27.

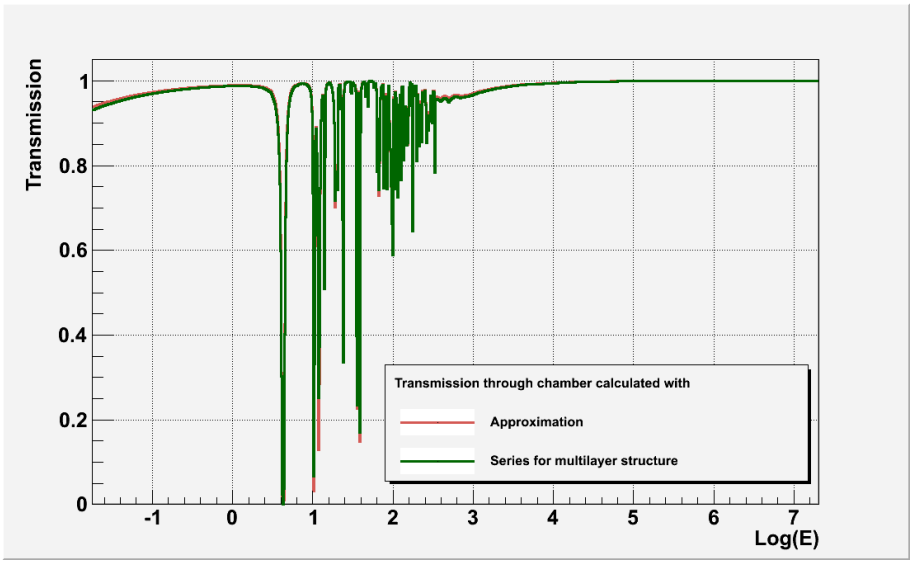


Figure 27: Comparison of the calculated transmission through the fission chamber, using (62) and (63).

6.4 Neutron fluence

The fission yield $Y(E_n)$ for the evaluation of the neutron fluence and the corrections for the present materials in the neutrons path has been calculated in three ways.
A Monte Carlo Simulation with the program MCNP, based on the detailed geometry of the radiation shielding container and the fission chamber itself has been performed by David Villamarin from CIEMAT (Spain).
The analytical approach was to calculate the fission yield using relation (50) and applying corrections for the materials in the neutron's flight path.
The analytical calculation has been performed once as exact as possible and with appropriate approximations on the other side.
After calculating the transmission T_i of neutrons through the given materials, the neutron fluence in isolethargic units can be obtained through the relation

$$\Phi = \frac{C}{Y \cdot \varepsilon \cdot \ln\left(\frac{E_{hi}}{E_{low}}\right) \cdot \sum_i T_i}, \tag{64}$$

where C are the counts of the detector at a certain time interval, E_{hi} and E_{low} are the borders of the corresponding energy interval, ε is the efficiency of the fission chamber and the index i stands for all the materials mentioned in the previous sections.
In Table 6 it is listed, for each of the three ways of evaluating the neutron fluence, how the contribution of the different materials has been obtained.

Correction for neutron losses in	Simulation	Analytical calculation	Analytical approximation
Air	T_{air}, Table 4	T_{air}, Table 4	T_{air}, Table 4
Al window	MCNP	T_{Al}, Table 5	T_{Al}, only ^{27}Al
Ta window	MCNP	T_{Ta}	T_{Ta}
Multilayer structure	MCNP	Eq. (62)	Eq. (63)
Reaction Yield calculated using	MCNP	Eq. (50), considering Table 56	Eq. (50), considering only ^{235}U

Table 6: Evaluation of the neutron fluence. The transmission values T_i have been calculated using Eq. (60) considering the materials mentioned next to it.

The fission cross section for the U deposit has been evaluated using the ENDF/B-VII.0

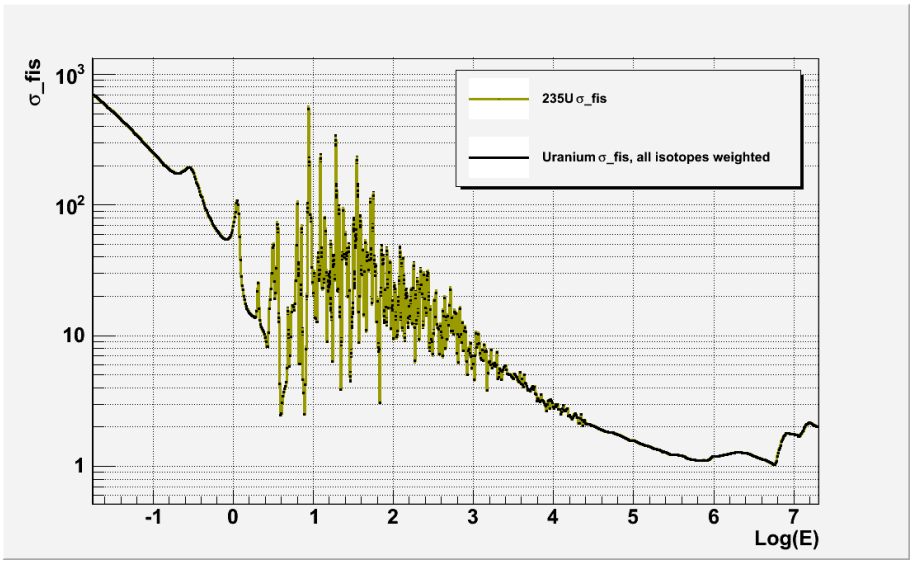


Figure 28: Comparison of σ_{fis} of ^{235}U and the U with impurities.

data for all the isotopes present in the deposits, weighted by the factors declared in reference [20] and listed in Table 56 respectively.
In Fig. 28 the fission cross section of pure ^{235}U is compared with the evaluated cross section for the U deposit in the detector.
In the resonance region the contribution of the other U isotopes can be seen. Below and above this region the cross sections are the same. It is valid to use the fission cross section of pure ^{235}U for the calculation of the reaction yield.

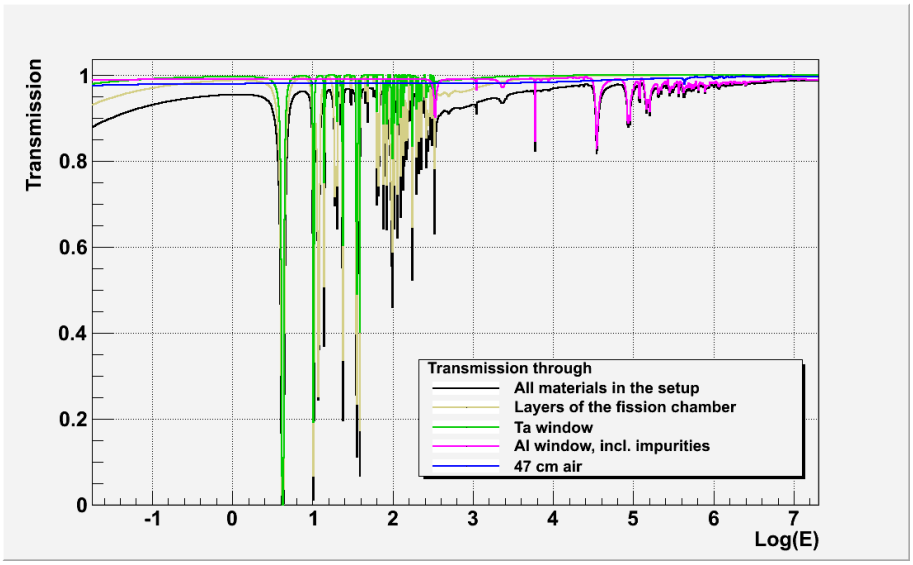


Figure 29: Corrections used in the exact analytical evaluation.

The sum of the corrections that need to be made for the presence of all the materials in the neutron's path before and within the fission chamber is plotted in Fig. 29. The black function shows the transmission as used in the exact analytical evaluation of the fluence.

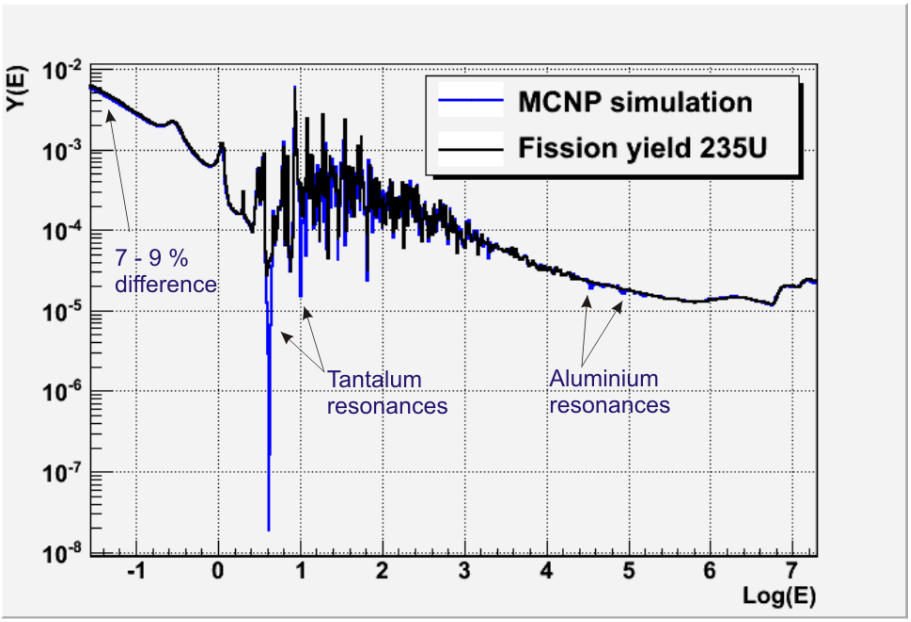


Figure 30: Comparison of the reaction yield gained by the Monte Carlo Simulation of the experimental setup with the reaction yield of pure ^{235}U.

In Fig. 30 the reaction yield obtained by the MCNP simulation is drawn in comparison to the fission yield of ^{235}U calculated using Eq. (50). The resonances of Al can be seen in the high energy region. The contribution of Ta and Pt are clearly visible in the resonance region.

At thermal energies the difference from the simulated to the calculated reaction yield is 7-9%. This is especially due to the multilayer structure of the fission chamber. Here the neutron absorption in Ta, Pt and U have a strong influence and can not be neglected. The Al window, although 1 mm thick, has in comparison a secondary effect.

The MCNP simulation did not consider the 47 cm air layer. The evaluated neutron fluence with the reaction yield of the simulation has to be corrected for this layer.

Due to considerations of work efficiency the fluence determination with the analytical approximation is to be preferred.

6.5 Results

The final neutron fluence results over the whole energy range, calculated in the previously specified three ways, are drawn in Fig. 31. Outside the resonance region they all agree in the order of magnitude and shape of the neutron fluence at n_TOF in the experimental area.

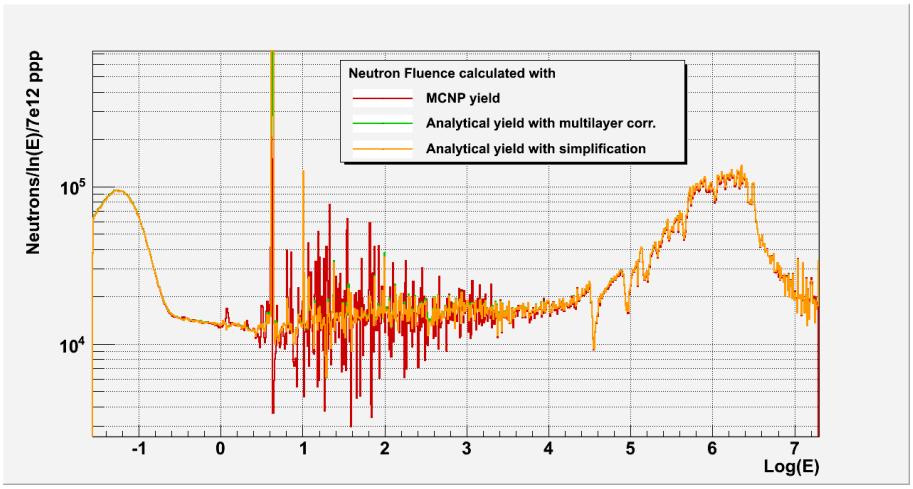


Figure 31: Calculated neutron fluence from thermal energies to 20 MeV. Results obtained by considering MCNP simulation in red, analytical calculation in green and the approximation in orange.

As for neutron capture cross section measurements the shape as well as the intensity of the incoming neutron fluence is important, the evaluation of these figures was a very important subject during the commissioning of the new neutron target of the n_TOF facility. The comparison with the results of the other methods used for determining the neutron fluence is made in Sec. 6.6.
The comparison to the neutron fluence of the old spallation target of the facility is discussed in Sec. 6.7.

Figure 32 shows a zoom into the low energy region of the obtained flux results. Below, the ratio between the neutron fluence obtained by the detailed calculation and by the MCNP simulation, as well as the ratio between the fluence calculated with the approximation and the MCNP simulation, are drawn.

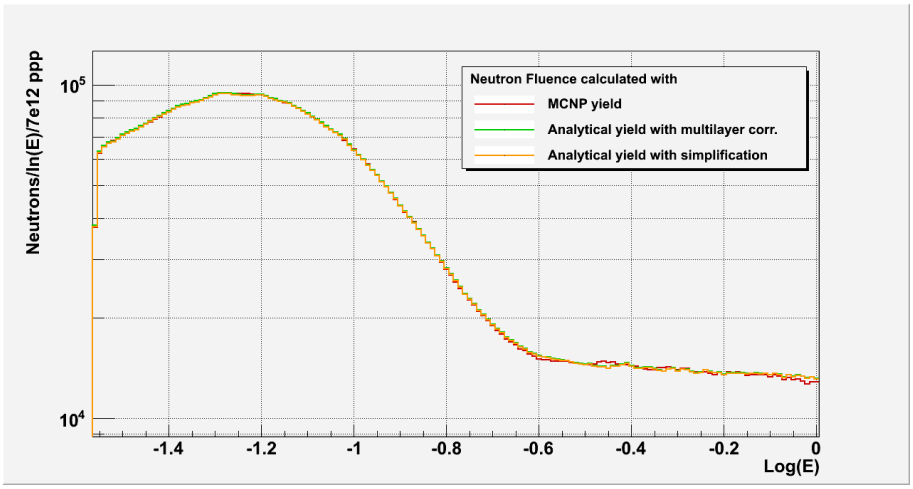


Figure 32: Neutron fluence in isolethargic units at low energies.

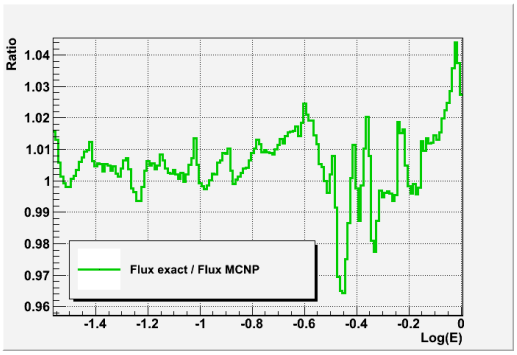


Figure 33: Ratio between multilayer and MCNP.

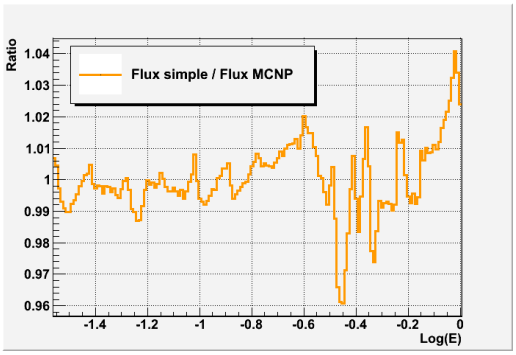


Figure 34: Ratio between approximation and MCNP.

The results at the lowest energies agree in both cases within one percent. The approximation is correcting less for the present materials in this energy range than the simulation and, as expected, the evaluation using (62). The absolute value of the approximation lies closer to the result of the simulation.

On integration over the low energy region the fluence resulting through the calculation with the approximation is 0.19% less than the fluence calculated with the MCNP simulation. The exact analytical calculation gives a neutron fluence 0.42% higher than the simulation.

Figure 35 shows a zoom into the high energy region of the obtained flux results. The ratio between the neutron fluence obtained by the detailed calculation and by the MCNP simulation, as well as the ratio between the fluence calculated with the approximation and the MCNP simulation, are drawn again below.

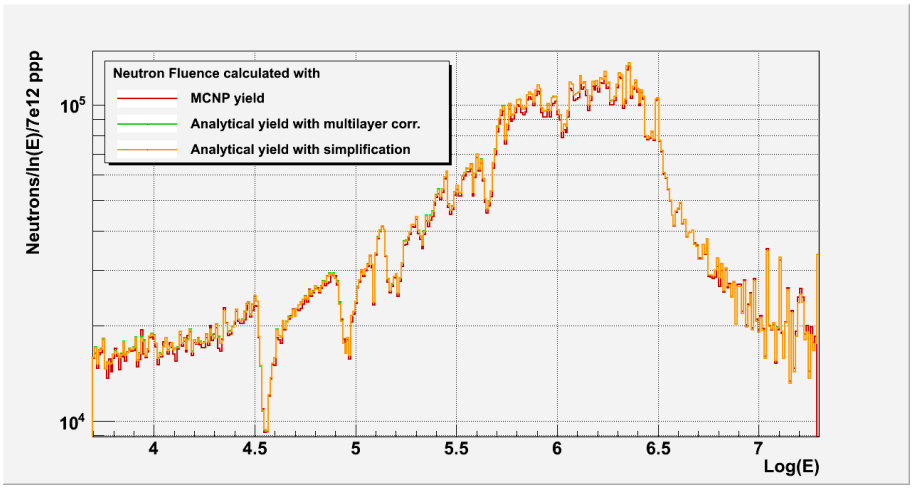


Figure 35: Neutron fluence in isolethargic units at high energies.

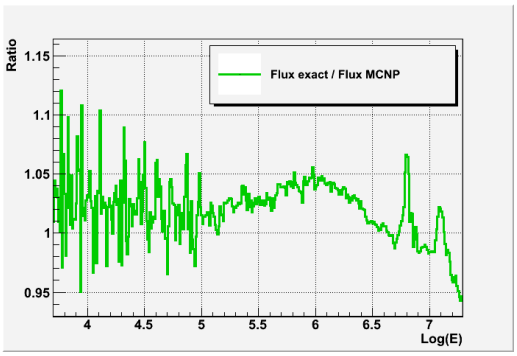


Figure 36: Ratio between multilayer and MCNP.

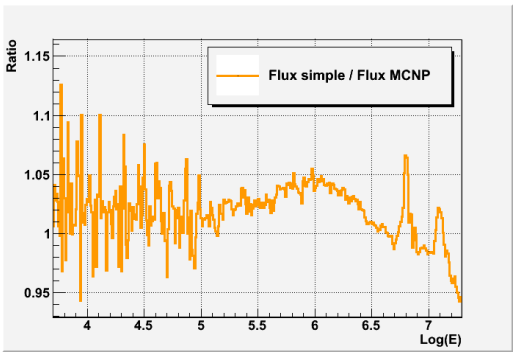


Figure 37: Ratio between approximation and MCNP.

The approximation lies closer to the result of the MCNP simulation. The analytical calculation of the transmission through the Al window results in a bigger neutron loss than the simulation predicts.

On integration over the high energy region the fluence resulting through the calculation with the approximation is 2.51% higher than the fluence calculated with the MCNP simulation.

The exact analytical calculation gives a neutron number of 2.6% more than the simulation.

6.6 Results from different detectors

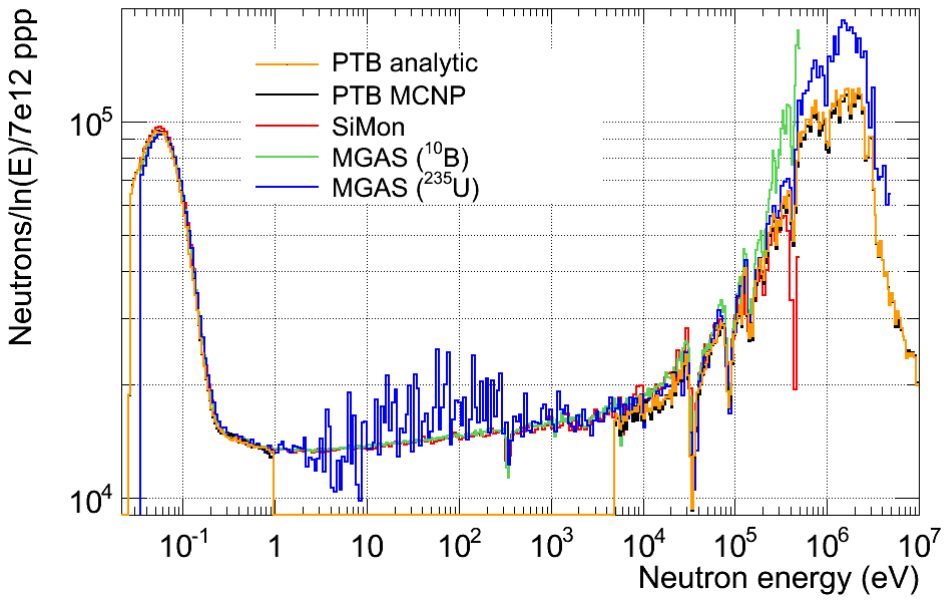


Figure 38: Comparison of the results of the fluence measurements with different detectors.

In Fig. 38 the results from the fluence measurements with the different detectors is compared. The orange curve is the result of the analytical flux determination with the fission chamber with following approximations:

- The impurities of the Al window as well as the impurities of the ^{235}U deposit have been neglected
- Only half of the amount of Ta, Pt and U within the chamber have been accounted for in the correction for these materials. This is equivalent to a single layer approximation with a window of each material in front of the detector's active area.

In the low energy region all the fluence measurements agree well within 1%.
In the high energy region the results of the Micromegas detector with the ^{235}U deposit is well above the results of the PTB fission chamber. The data taken with the Micromegas detector is greatly affected by the uncertainty on the beam interception. As stated already, there have been difficulties with the alignment of this detector during the commissioning. Given the uncertainties in the position of the detector and the associated beam interception factor, which is strongly energy dependent, the discrepancies are understandable and the result of the PTB fission chamber is to be trusted.
In the analysis of the data given by the Micromegas detector with the ^{10}B deposit it has to be taken into account that above a few tens of keV recoiled protons start to increase

the uncertainty of the measurement. The plotted data is not corrected for this effect. The higher fluence given by the $MGAS_{^{10}B}$ detector in the keV region is therefore explainable. Additionally ^{10}B is a standard just up to 200 keV and the fluence results above this energy can not be taken into account for the determination of the final fluence.
The differences between the silicon monitor data and the PTB fission chamber data in the region from 5-12 keV can be related to the uncertainty of the geometric efficiency ε of the SILI. According to Carlos Guerrero, who has evaluated the data for this detector, the signal amplitude of the four silicon detectors indicated a misalignment for this detector. In fact, there has been a misalignment of the second collimator in the experimental setup at n_TOF in 2009. This resulted in the misalignment of the neutron beam with the silicon monitor. Only through a Monte Carlo simulation, including the exact geometry, ε can be determined. As the misalignment could not be taken into account in the simulation of ε, there is an uncertainty associated with this quantity and therefore the obtained fluence results.
The final shape and the intensity of the neutron flux for the experimental runs 2009 will be given by a combination of the data taken with the PTB fission chamber (below 1 eV and above 5 keV), the data from $MGAS_{^{10}B}$ (below 100 keV) and Monte Carlo simulations (above 5 keV), which will be performed using the programs FLUKA and MCNP by members of the n_TOF collaboration.

6.7 Neutron fluence, old versus new target

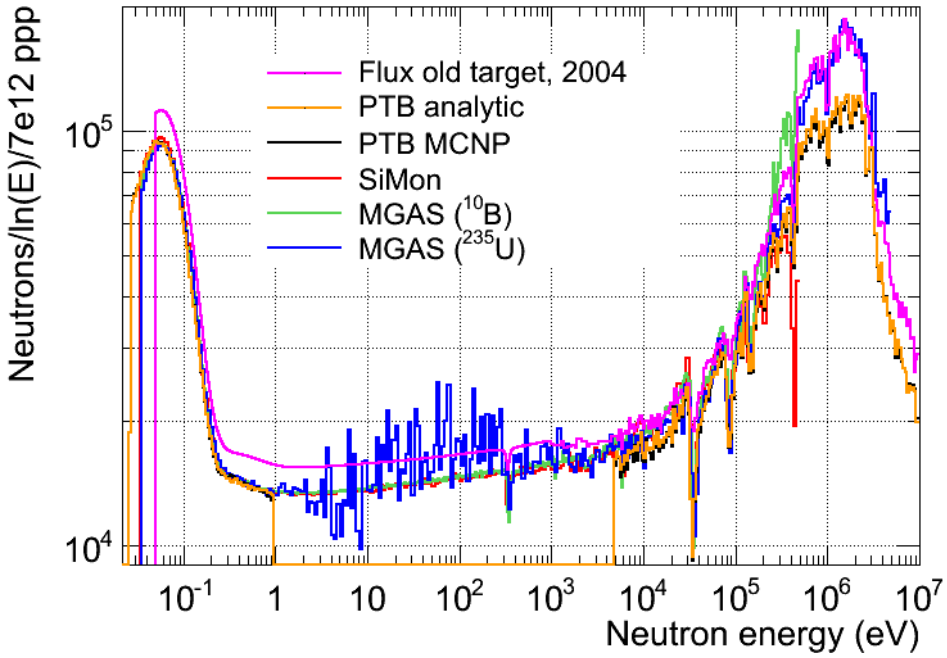


Figure 39: Comparison of the experimental results with the neutron fluence of the old target, measured 2004.

In Fig. 39 the neutron fluence results from the commissioning of the old spallation target at n_TOF 2004 is plotted in comparison with all the experimental data of the commissioning of the new target in 2009. It can be clearly seen that there is a difference in the intensity over the whole range. On average the difference is 17%. The shape of the neutron fluence between old and new spallation target is comparable.
A simulation of the expected neutron fluence of the new target has been performed by the group of Vasilis Vlachoudis at CERN with the simulation program FLUKA. This simulation gave an expected intensity of the neutron beam about 20% higher than the experimental results of the commissioning show. As an improvement of the statistics of this simulation is needed, the data is not included in the evaluation for this thesis.
There was an investigation in november 2009 on the alignment of the second collimator of the facility. There were several indications for a misalignment:

1. The experimental neutron fluence was much lower than the simulated one
2. The beam profile, which was measured with a position sensitive Micromegas detector, showed an asymmetry in the vertical direction
3. The data taken with the silicon detector showed a misalignment with the beam

A tilt of -2 mm in the collimator has resulted in a 11% increase of the neutron fluence.

7 Experiment on neutron absorption in air

At the TRIGA Mark II reactor in the Atomic Institute of the Austrian Universities (ATI) a TOF experiment has been performed in order to find out if the condition (39) for strongly bound atoms also applies to a molecular gas like air.

7.1 Experimental setup

The neutron transmission through a steel tube, 111 cm in length with an inner diameter of 4 cm, has been measured. This measurement volume was alternately

- Evacuated to 10^{-4} bar
- Filled with air at atmospheric pressure.

The experimental setup can be seen in Fig. 40.

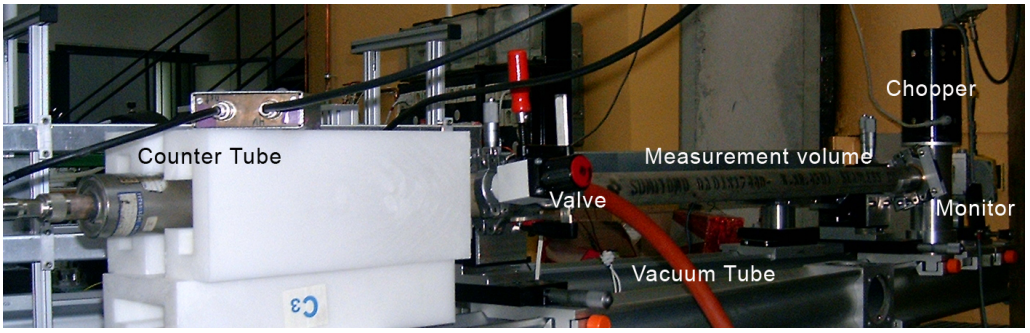


Figure 40: Experimental setup at the TRIGA Mark II reactor.

Upstream of the neutron beam a fission chamber was mounted as monitor for the incoming neutrons. As the neutron yield of the reactor cannot be assumed to be constant over a day, and especially over a whole week, the experimental data has been normalized to the monitor counts.
The beam chopper was installed behind a Cd window of variable size. The window was necessary to reduce the background of the experiment to a minimum. A close picture of the front end setup of the experiment can be seen in Fig. 41.
The steel tube was mounted on two adjustable supports. At both ends the tube was closed with Al windows and a borated ring with an inner diameter of 3 cm was mounted in order to conduct the neutrons through the inside of the tube and reduce the influence of the

tube's wall on the experiment.
The evacuation of the tube was done with a rotary vane pump to $(2 \pm 0.5) \cdot 10^{-4}$ bar. This is sufficient for the implemented experiment.
For the neutron detection at the end of the tube a cylindrical BF_3 counter, 36 cm in length with an entrance window of 5 cm in diameter, has been used. It was mounted in between bricks made from borated polyethylene to shield it from additional background.

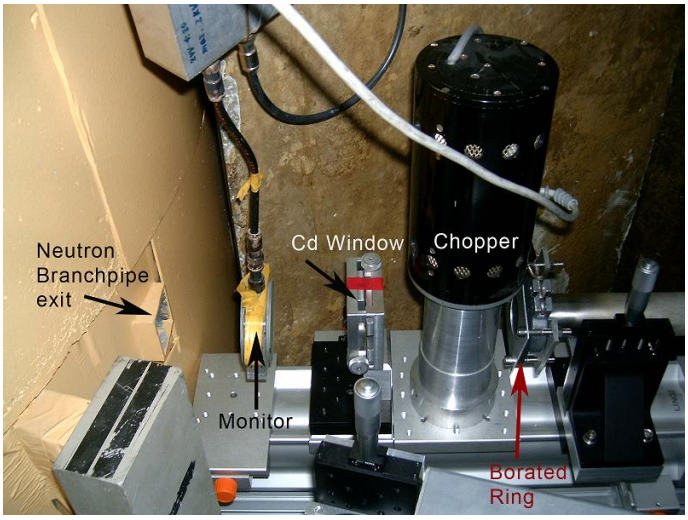


Figure 41: Experimental setup close to the neutron beam tube exit window.

The transmission is energy dependent and for the experiment at the ATI it had to be evaluated which energy the provided neutrons have. The neutron beam coming out of the reactors core has a white spectrum. The neutrons get diffracted at a crystal according to Bragg's law

$$2d_{hkl} \sin \Theta = n\lambda. \tag{65}$$

Neutrons with the wavelength λ get diffracted in the direction of the angle Θ. This is the wavelength of the first order as $n = 1$. Neutrons with the wavelengths $n\lambda$ with $n = 2, 3, ..$ will be detected at the same angle.
The recorded time of flight spectra at the experiment where not normalized to $t = 0$. The TOF of the outcoming neutrons was evaluated using the maximum of the distributions of the 1. and 2. order neutrons. From the relation for the de Broglie wavelength

$$\lambda = \frac{h}{p} = \frac{h}{mv} \tag{66}$$

it is evident that the velocity v of the second order neutrons must be twice the velocity of the first order neutrons.
The recorded spectra showed that $\Delta\text{TOF} = (270 \pm 2)$ μs and TOF(1.Order) $= (540 \pm 4)$ μs.

Through the geometry of the setup at the TRIGA Mark II reactor, the beam tube used for the experiment provides neutrons with a wavelength of $\lambda_1 = 1.66$ Å in the first order. Neutrons of the second and third order, with $\lambda_2 = 0.83$ Å and $\lambda_3 = 0.55$ Å respectively, could also be distinguished in the spectra, see exemplary experimental data in Fig. 42. The intensity of the first and second order neutrons is sufficient to be taken into the experimental evaluation. The associated energy of the neutrons is

$$1.\text{Order} \qquad \lambda_1 = 1.66 \text{ Å} \qquad E_n = 0.03 \text{ eV} \tag{67}$$

$$2.\text{Order} \qquad \lambda_2 = 0.83 \text{ Å} \qquad E_n = 0.12 \text{ eV} \tag{68}$$



Figure 42: Spectrum from transmission experiment with vacuum at TRIGA Mark II reactor, ATI. The colored areas indicate the integration interval. The background line fit for each interval is quoted above in a text box.

The recorded background was fitted with a constant line in each of the three regions. To receive the total counts the TOF data were integrated over an area including the peak, see Fig. 42. The background was averaged taking the linear fit on either side of the peak and deducted from the integral. The number of counts n received in this way was finally divided by the detected number of monitor neutrons n_m during the experimental run.

7.2 Calculation of the transmission

The transmission T through the air layer was evaluated according to the principles mentioned in Sec. 3.2. The composition of dry air was taken as listed in Table 7. Trace gases like CO_2, O_2 and others have been neglected in the calculation.

The air temperature, relative atmospheric moisture and atmospheric pressure in the reactor hall were monitored during the experimental runs. The data is listed in Sec. 9.2.

Molecule	Isotope	Vol%
N_2	^{14}N	78.12
O_2	^{16}O	20.95
Ar	99.6% ^{40}Ar	0.93
	0.4% ^{36}Ar	

Table 7: Assumed composition of dry air.

As the conditions over each experimental run were stable enough, the mean value of each of these figures was taken in the calculation of the transmission. With these values the volume % of H_2O in air and the density of air has been evaluated. Finally the Vol% of the other molecules were changed accordingly.
The resulting values for absorption in air lie all within the error margins quoted in Table 8. The cross section data was taken from the ENDF/B-VII.0 database. The listed scattering cross section data in this database corresponds to σ_s(free). σ_s(bound) was calculated using relation (40).

7.3 Results

Vacuum and Air at atmospheric pressure have been measured on 4 different days. Each experimental run had a duration of 20 minutes.
The data of the environmental conditions over the measurement period, the monitor counts and the evaluated total counts for the neutrons of the first and second order are listed in Sec. 9.2.
The counting rates of different experimental days are not compatible. This could be due to the alignment of the experimental setup. During one day the alignment has not been changed. Minor adjustments have been performed before starting the experimental periods.
That the results of different days differ could also point to systematic errors in the experiment which have not been recognized yet.
A possible systematic error of the experiment comes from the neighbouring beam tube. When it is in use, it is likely that additional background is present. The status of this beam tube has not been monitored during the experimental campaign.
The consistency of the experimental data related to the first and second order neutrons differs (as example see air measurements of 3.3.2010, Sec. 9.2). This is likely due to the smaller counting rates for the second order neutrons. Longer measurement times would minimize the influence of this statistical error. Additionally this would reduce the statistical error made through the background fit.

In Table 8 the evaluated transmission of neutrons through air for each experimental day is listed. The corresponding absorption as well as the calculated values for the absorption are listed below the experimental data.

Transmission [%]	Date	Transmission [%]
2.Order: $\lambda = 0.8$ Å $E = 0.12$ eV		1.Order: $\lambda = 1.7$ Å $E = 0.03$ eV
(95.54 ± 1.29) % (95.58 ± 0.83) % (96.23 ± 1.09) % (96.09 ± 2.42) %	3.3.2010 4.3.2010 5.3.2010 9.3.2010	(94.72 ± 0.65) % (93.72 ± 0.48) % (94.87 ± 0.74) % (94.97 ± 0.59) %
(95.86 ± 1.53) %	Transmission Mean value	(94.57 ± 0.62) %
(4.14 ± 1.53) %	Absorption	(5.43 ± 0.62) %
Expected Absorption	calculated with	Expected Absorption
(5.02 ± 0.02) %	$\sigma_{tot} = \sigma_a + \sigma_s$(free)	(5.48 ± 0.02) %
(5.77 ± 0.03) %	$\sigma_{tot} = \sigma_a + \sigma_s$(bound)	(6.28 ± 0.04) %

Table 8: Experimental results and theoretical calculation of the neutron absorption in air

The expected values for the absorption, when calculated with $\sigma_{tot} = \sigma_a + \sigma_s$(free), lie closer to the experimental results. The errors σ quoted for the experimental results are calculated after the principles of error propagation. As both calculated values lie within 2σ the result of the experiment is at this point not significant.
It is suggested to repeat the experiment. The following points should be implemented:

1. In order to reduce the influence of statistical errors the duration of each experimental run should be increased.
2. The alignment of the setup should be optimized to a maximum count rate of the detector at the beginning of the experimental campaign.
3. In order to get compatible data between the days, this alignment should not be altered after the initial adjustments.
4. The status of the neighbouring beam tube should be monitored to exclude this potential systematic error.

8 Summary

8.1 Neutron fluence at n_TOF 2009

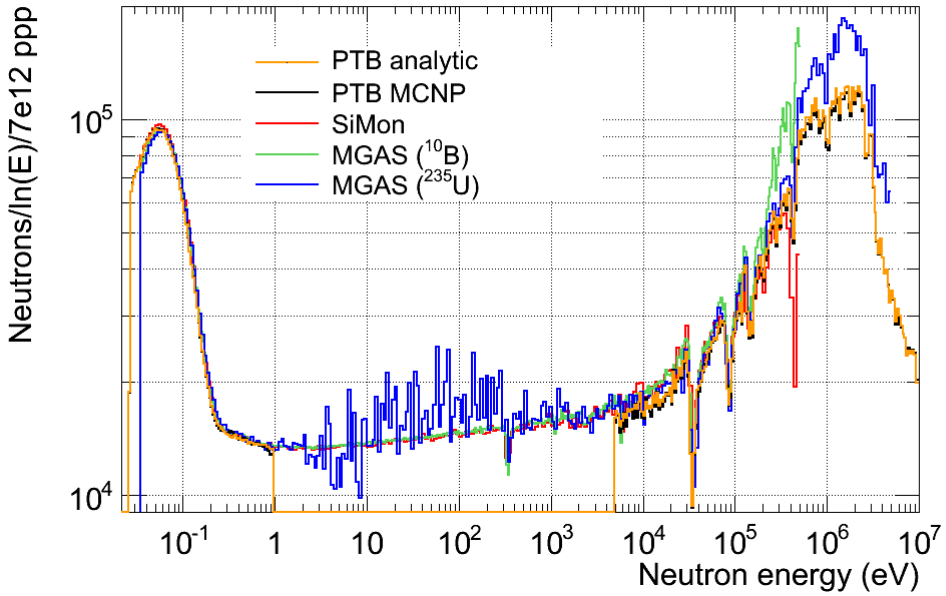


Figure 43: Comparison of the results of the fluence measurements with different detectors.

For the neutron fluence measurement at the commissioning of the new spallation target of n_TOF in 2009, amongst others, a fission chamber of PTB Braunschweig has been used. For the determination of the fluence, the reaction yield $Y(E_n)$ has been evaluated in three different ways. The details are listed in Table 6. The analytical approach with the mentioned approximations gives a satisfying result.
In Fig. 43 the results of the fluence measurements performed with different detectors are plotted. The differences in the intensity of the fluence are understandable through the error estimations given in Sec. 6.6.
The final shape and the intensity of the neutron fluence for the experimental runs of 2009 will be given by a combination of the data taken with the PTB fission chamber (below 1 eV and above 5 keV), the data from $MGAS_{^{10}B}$ (below 100 keV) and Monte Carlo simulations (above 5 keV), which will be performed using the programs FLUKA and MCNP by members of the n_TOF collaboration.
The experimental results of the neutron fluence determination are about 20% less than the simulated intensity of the neutron beam. This is due to a misalignment of the second collimator during the commissioning and the experimental period at n_TOF 2009.

8.2 Experiment on neutron absorption in air

A transmission experiment has been performed at the TRIGA Mark II reactor of the Atomic Institute of the Austrian Universities (ATI). The aim of the experiment was to find out if relation (39) applies to the molecular bonds in air and if the scattering cross section for strongly bound atoms in Eq. (40) has to be taken into account in the calculation for the neutron losses in air at n_TOF.
The detailed experimental data is listed in Sec. 9.2. The final results of the experiment are quoted in Table 9.

Incident Neutron Energy	Experimental Result for Absorption	Calculated Absorption	Absorption calculated with
0.03 eV	(5.43 ± 0.62) %	(5.48 ± 0.02) %	$\sigma_{tot} = \sigma_a + \sigma_s(\text{free})$
		(6.28 ± 0.04) %	$\sigma_{tot} = \sigma_a + \sigma_s(\text{bound})$
0.12 eV	(4.14 ± 1.53) %	(5.02 ± 0.02) %	$\sigma_{tot} = \sigma_a + \sigma_s(\text{free})$
		(5.77 ± 0.03) %	$\sigma_{tot} = \sigma_a + \sigma_s(\text{bound})$

Table 9: Experimental results of the transmission experiment at the ATI. The length of the air layer was 111 cm.

The comparison of the experimental results and the absorption values given by the calculations show that the experimental results lie closer to the calculation of the absorption performed with $\sigma_{tot} = \sigma_a + \sigma_s(\text{free})$. This justifies that the cross sectional data for the materials at n_TOF is taken from the ENDF/B-VII.0 database, which has $\sigma_s(\text{free})$ listed for all the isotopes.
Still, the standard deviation of the experimental results is too big to make a concrete conclusion. It is proposed to repeat the experiment at the ATI with attention to the suggestions in Sec. 7.3.

References

[1] *http://www.nndc.bnl.gov/.*

[2] C. Iliadis, *Nuclear Physics of Stars.* Wiley-VCH, 2007.

[3] Nuclear Energy Agency NEA, *Accelerator-driven Systems (ADS) and Fast Reactors (FR) in Advanced Nuclear Fuel Cycles.* OECD, 2002.

[4] C. Rubbia et al., *A high Resolution Spallation driven Facility at the CERN-PS to measure Neutron Cross Sections in the Interval from 1 eV to 250 MeV.* CERN/LHC/98-02 (EET), (1998).
C. Rubbia et al., *A high Resolution Spallation driven Facility at the CERN-PS to measure Neutron Cross Sections in the Interval from 1 eV to 250 MeV.* CERN/LHC/98-02 (EET)-Add.1, (1998)

[5] The n_TOF collaboration, *n_ TOF New target commissioning and beam characterization.* EUROPEAN ORGANIZATION FOR NUCLEAR RESEARCH, Proposal to the ISOLDE and Neutron Time-of-Flight Committee.

[6] The n_TOF Collaboration, *Determination of the neutron fluence, the beam characteristics and the backgrounds at the CERN-PS TOF Facility.* CERN/INTC 2000-016, 2000.

[7] G. Lorusso et al., *Time-energy relation of the n_ TOF neutron beam: energy standards revisited.* Nucl. Instr. and Meth. in Phys. Res. A 532 (2004), p. 622.

[8] L.F.Curtiss, *Introduction to Neutron Physics.* D.van Nostrand Company, Inc., 1959.

[9] K.Wirtz and K.H.Beckurts, *Elementare Neutronenphysik.* Springer-Verlag, 1958.

[10] V.F.Sears, *Neutron Optics.* Oxford University Press, 1989.

[11] M. Sowerby, in *Nuclear Data Standards For Nuclear Measurements.* NEA OESD, 1992, p. 51.

[12] H. Tellier, in *Nuclear Data Standards For Nuclear Measurements.* NEA OESD, 1992, p. 90.

[13] G.M.Hale and P.G.Young, in *Nuclear Data Standards For Nuclear Measurements.* NEA OESD, 1992, p. 22.

[14] E.Wattecamps, in *Nuclear Data Standards For Nuclear Measurements.* NEA OESD, 1992, p. 27.

[15] S. Andriamonje et al., *A new detector for neutron beam monitoring.* http://www-pub.iaea.org/MTCD/publications/PDF/P1433_CD/datasets/papers/at_oc-02.pdf, AT/OC-02.

[16] S. Andriamonje et al., *New neutron detectors based on Micromegas technology.* Nucl. Instr. and Meth. in Phys. Res., A 525 (2004) 74-78.

[17] S.Marrone et al., The n_TOF collaboration, *A low background neutron flux monitor for the n_ TOF facility at CERN.* Nucl. Instr. and Meth. in Phys. Res., A 517 (2004) 389-398.

[18] V.Lacoste, et al., *Neutron flux measured by activation of gold foils during the commissioning of the n_ TOF facility.* CERN/SL/EET Internal Note 2001-004, 2001.

[19] C.Guerrero et al., The n_TOF collaboration, *The n_ TOF Total Absorption Calorimeter for neutron capture measurements at CERN.* Nucl. Instr. and Meth. in Phys. Res., A 608 (2009) 424-433.

[20] D. B. Gayther, *International Intercomparison of Fast Neutron Fluence-Rate Measurements Using Fission Chamber Transfer Instruments.* Springer, Metrologia 27, 221-231 (1990).

[21] E.Browne, *Nuclear Data Sheets 93, Web: www.nndc.bnl.gov.* 986 (2001).

[22] *http://www.kayelaby.npl.co.uk/atomic_ and_ nuclear_ physics/4_ 7/4_ 7_ 1a.html.*

List of Figures

1 Chart of nuclides, after [1]. The colour code indicates the different half lives of the isotopes. Isotopes with a half life greater than 10^{15} seconds are marked in dark blue. Up to the mark of 82 protons and 126 neutrons the so called "valley of stability" follows this dark blue line. 6

2 Zoom into the chart of nuclides. The s-process path is shown with solid lines, the r-process with dotted lines. Indicated below each stable isotope is the process responsible for it's creation. 7

3 Cross sections of ^{239}Pu against the energy of the incident neutrons, after [1]. The fission cross section is drawn in green, the capture cross section in red. The blue curve, approximately the sum of the two, is the total cross section of ^{239}Pu. 9

4 n_TOF facility layout at CERN. 10

5 Cut through a model of the new spallation target at the n_TOF facility, after [5]. 12

6 Cross sections of ^{14}N against the energy of the incident neutrons, after [1]. The scattering cross section σ_s is drawn in green, the capture cross section σ_a in red. The blue curve is the total cross section σ_{tot} of ^{14}N. 20

7 $\frac{\sigma_s(\text{bound})}{\sigma_s(\text{free})}$ versus mass number A. 22

8 Developed Micromegas detector; working principle, after [16], on the left and design, after [15], on the right. 27

9 Schematic view of the silicon monitor, after [17]. 28

10 Opened 4π Total Absorption Calorimeter; in the middle the spherical neutron absorber/moderator for reducing the background from scattered neutrons can be seen. 30

11 Schematic drawing of the fission chamber, the ^{235}U deposits are drawn in yellow. 33

12 Fission cross section of ^{235}U, after [1]. 34

13 Fission product yield of different materials, after [22]. 35

14 Original experimental setup with the PTB chamber. The Micromegas detector was removed, leaving 47 cm of air between the silicon detector and the radiation shielding of the PTB chamber. 36

15 Original setup with silicon monitor, Micromegas detector and PTB chamber, inside the radiation protection container, behind each other at the commissioning. 38

16 Comparison of the time of flight spectra from runs with and without the MGAS detector in front of the fission chamber. 39

17 Experimental data 39

18 Relative error of the experimental data in %. 40
19 Background measurement of the PTB chamber. 40
20 Pulse height distribution of the data from detector 1. 41
21 Pulse height distribution of the data from detector 3. 41
22 Correction factor for 47 cm of air, calculated with $\sigma_{(n,tot)}$ in blue and with $\sigma_{(n,\gamma)}$ in red. 43
23 Radiation protection container with the PTB fission chamber and TAC in the experimental area. 44
24 Correction factor for the Al window in blue. In comparison the correction for pure ^{27}Al is shown in red. 45
25 Correction for the Ta window. 46
26 Schematic view of the fission chamber with all layers. Ta electrodes in magenta, Pt electrodes in blue, and U layers in yellow. The incident neutron flux is described below for the second, the fifth and the last U layer. 47
27 Comparison of the calculated transmission through the fission chamber, using (62) and (63). 48
28 Comparison of σ_{fis} of ^{235}U and the U with impurities. 50
29 Corrections used in the exact analytical evaluation. 50
30 Comparison of the reaction yield gained by the Monte Carlo Simulation of the experimental setup with the reaction yield of pure ^{235}U. 51
31 Calculated neutron fluence from thermal energies to 20 MeV. Results obtained by considering MCNP simulation in red, analytical calculation in green and the approximation in orange. 52
32 Neutron fluence in isolethargic units at low energies. 53
33 Ratio between multilayer and MCNP. 53
34 Ratio between approximation and MCNP. 53
35 Neutron fluence in isolethargic units at high energies. 54
36 Ratio between multilayer and MCNP. 54
37 Ratio between approximation and MCNP. 54
38 Comparison of the results of the fluence measurements with different detectors. 55
39 Comparison of the experimental results with the neutron fluence of the old target, measured 2004. 57
40 Experimental setup at the TRIGA Mark II reactor. 59
41 Experimental setup close to the neutron beam tube exit window. 60
42 Spectrum from transmission experiment with vacuum at TRIGA Mark II reactor, ATI. The colored areas indicate the integration interval. The background line fit for each interval is quoted above in a text box. 61
43 Comparison of the results of the fluence measurements with different detectors. 64

44 Scattering geometry in the laboratory system. R is the distance between the interaction point and the detector, r is the radius of the active area of the detector. 74

List of Tables

1 Configuration of the three data acquisition channels of the fission chamber. 36
2 Materials in the neutron flight path in the experimental area, before and within the PTB fission chamber. The calculated neutron flux needs to be corrected for the losses of neutrons through the interactions with these materials. . . . 37
3 Experimental runs that are not taken into account in the data analysis for the quoted reasons. . . . 38
4 Composition of air as assumed in the calculation. . . . 42
5 Contents of the Al window of the radiation shielding container. . . . 44
6 Evaluation of the neutron fluence. The transmission values T_i have been calculated using Eq. (60) considering the materials mentioned next to it. . . . 49
7 Assumed composition of dry air. . . . 62
8 Experimental results and theoretical calculation of the neutron absorption in air . . . 63
9 Experimental results of the transmission experiment at the ATI. The length of the air layer was 111 cm. . . . 65
10 Values for integration in each of the cases. . . . 75
11 Experimental data of environmental conditions, 3.March 2010. . . . 76
12 Experimental data of neutron monitor, 3.March 2010. . . . 76
13 Experimental Data, 3.March 2010. . . . 76
14 Experimental data of environmental conditions, 4.March 2010. . . . 77
15 Experimental data of neutron monitor, 4.March 2010. . . . 77
16 Experimental Data, 4.March 2010. . . . 77
17 Experimental data of environmental conditions, 5.March 2010. . . . 78
18 Experimental data of neutron monitor, 5.March 2010. . . . 78
19 Experimental Data, 5.March 2010. . . . 78
20 Experimental data of environmental conditions, 9.March 2010. . . . 79
21 Experimental data of neutron monitor, 9.March 2010. . . . 80
22 Experimental Data, 9.March 2010. . . . 80

9 Appendix

9.1 Error calculations

Nuclear reactions, being stochastic processes, underlie the Poisson statistics. As an example, looking at the natural radioactive decay of a material, the probability $P_n(t)$ that, at a time t, n radioactive decays happened is equal to

$$P_n(t) \;=\; \frac{1}{n!}(\lambda t)^n \mathrm{e}^{-\lambda t}, \tag{69}$$

which is exactly the Poisson distribution. The decay constant λ is the expected value of the distribution.
When dealing with random variables in an experiment, such as a counting experiment, the data also underlies the Poisson statistics. If λ is the expected value of Poisson distributed variables, which is the mean value of a counting experiment, the root mean square deviation is

$$\sigma \;=\; \sqrt{\lambda}. \tag{70}$$

68% of the variables will lie within the interval of $(\lambda \pm \sigma)$. 95% are within 2 standard deviations and 99.7% will lie within the interval $(\lambda \pm 3\sigma)$ according to the empirical rule of statistics.
The variance, beeing σ^2, is equal to λ.
Out of relation (70) it becomes clear that, if the measured quantity has to have an error less than 0.1%, a counting rate of at least 10^6 has to be accomplished.

9.1.1 Error propagation

If a quantity f and its error Δf should be evaluated through the experiment, with

$$f \;=\; f(x,y,z) \;=\; f(x_i), \tag{71}$$

than the errors of the variables measured, Δx_i, have to be taken into account in the calculation of Δf. The biggest error made is calculated through

$$\Delta f \;=\; \left|\frac{\partial f}{\partial x}\right|\Delta x + \left|\frac{\partial f}{\partial y}\right|\Delta y + \cdots \;=\; \sum_{i=1}^{n}\left|\frac{\partial f}{\partial x_i}\right|\Delta x_i. \tag{72}$$

The mean absolute error of the quantity f, if the variables x_i are independent from each other, is given, after the error propagation law of Gauss, by

$$\Delta f = \sqrt{\left(\frac{\partial f}{\partial x}\Delta x\right)^2 + \left(\frac{\partial f}{\partial y}\Delta y\right)^2 + \left(\frac{\partial f}{\partial z}\Delta z\right)^2}. \quad (73)$$

If f is given of the form $f = x^a y^b \frac{1}{z^c}$, than $\Delta f/f$ becomes through Eq. (72)

$$\frac{\Delta f}{f} = |a|\frac{\Delta x}{x} + |b|\frac{\Delta y}{y} + |c|\frac{\Delta z}{z}. \quad (74)$$

The error propagation after Eq. (73) will then be given by

$$\frac{\Delta f}{f} = \sqrt{a^2\left(\frac{\Delta x}{x}\right)^2 + b^2\left(\frac{\Delta y}{y}\right)^2 + c^2\left(\frac{\Delta z}{z}\right)^2}. \quad (75)$$

In the evaluation of the experimental data the determination of the errors was performed according to these rules. Standardized data, like the data taken for the cross sections of the materials, where accepted as absolute. Therefore no error has been associated with it. The systematic errors made in the evaluation of the experimental data are discussed in the next section.

9.1.2 Scattering cross section

The calculated flux for n_TOF has been corrected for the losses in all materials before and within the fission chamber. For the air layer and the Al window the absorption as well as the scattering cross sections of the materials were taken into account. The same procedure has been chosen for the transmission experiment at the TRIGA Mark II reactor.
It has to be estimated how many of the scattered neutrons actually do end up in the detector and the calculated neutron losses have to be minimized by that factor.
The scattering of neutrons in the described experiments can be seen as isotropic, meaning no solid angle is preferential. In order to calculate the percentage of scattered neutrons who still get directed towards the fission chamber, the area of the detector has to be projected onto a sphere encircling the interaction point, see Fig. 44.
The ratio X between the projected detector area A_{det} and the surface area of the whole sphere A_{sph} gives the ratio between scattered neutrons which end up in the detector and the total number of scattered neutrons.
$A_{det} = 2\pi hR$ is obviously the surface area of the pink spherical cap in Fig. 44 which is smaller than the area of the detector. For big R it becomes equal to the surface area of the ^{235}U layers.

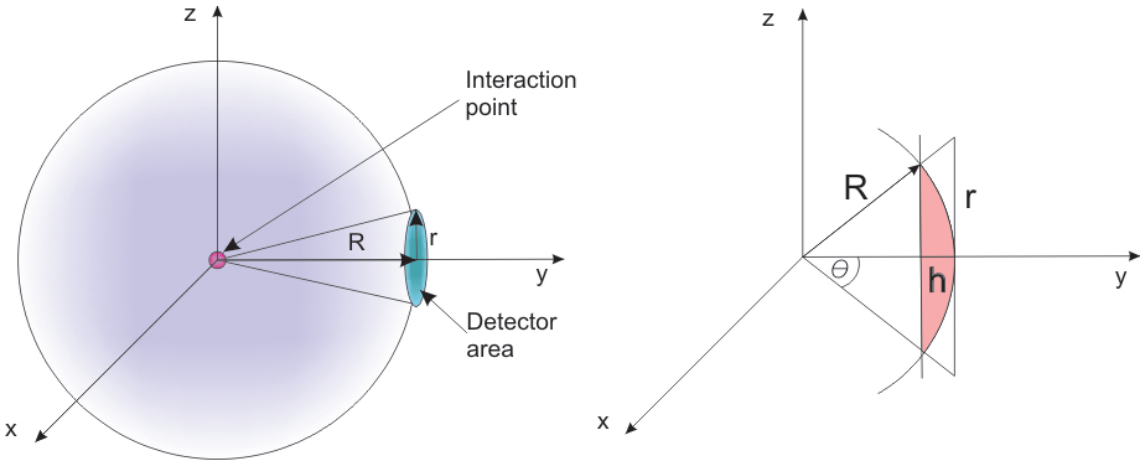


Figure 44: Scattering geometry in the laboratory system. R is the distance between the interaction point and the detector, r is the radius of the active area of the detector.

$$X = \frac{2\pi R^2[1-\cos(\arctan(\frac{r}{R}))]}{4\pi R^2} = \frac{1}{2}\left[1-\cos\left(\arctan\left(\frac{r}{R}\right)\right)\right] \tag{76}$$

The radius of the sphere R is the distance from the interaction point to the ^{235}U layers in the fission chamber.
Based on the experimental setup with the fission chamber, R is the sum of a constant factor R_0 and a variable distance ϱ. R_0 is given by the sum of the thickness of the aluminium window of the radiation shielding (0.1 cm), the distance between this window and the detector (4.4 cm) and half of the length of the fission chamber (2.5 cm). This gives in total a value of $R_0 = 7$ cm.
The radius of the ^{235}U layers in the fission chamber is $r = 3.5$ cm.
Along the $L = 47$ cm of air the scattering is equally likely at each position, meaning that the probability for scattering is not dependent on ϱ. To calculate the error ε made through the assumption that scattered neutrons are not available for detection anymore, X has to be integrated over ϱ and normalized to L.

$$\begin{aligned}
\varepsilon &= \int_a^b \frac{1}{2L}\left[1-\cos\left(\arctan\left(\frac{r}{R_0+\varrho}\right)\right)\right]\,\mathrm{d}\varrho \\
&= \frac{1}{2L}\int_a^b \left[1-\frac{1}{\sqrt{1+\left(\frac{r}{R_0+\varrho}\right)^2}}\right]\,\mathrm{d}\varrho \\
&= \frac{1}{2L}\left[\varrho - \frac{r^2+(R_0+\varrho)^2}{(R_0+\varrho)\sqrt{1+\frac{r^2}{(R_0+\varrho)^2}}}\right]\Bigg|_a^b
\end{aligned} \tag{77}$$

In the analysis of the experimental data the scattering cross section of a given material has been taken into account in three different cases. The correction regarding the air and the Al window at n_TOF and the calculation for the neutron losses in air for the experiment at the atomic institute considered σ_s.
The geometry in Fig. 44 applies to all three cases. The values for the constants in Eq. (77) and the resulting ε for each of these cases are listed in Table 10.
The results in Table 10 show that including the scattering cross section in the calculation

	n_TOF Air	n_TOF Al window	TRIGA Mark II Air
a[m]	0	0	0
b[m]	0.47	0.001	1.11
L[m]	0.54	0.07	1.29
r[m]	0.035	0.035	0.015
R_0[m]	0.07	0.069	0.18
ε	0.758e-2	5.343e-2	0.024e-2

Table 10: Values for integration in each of the cases.

of the losses in air is valid in both cases. The error made is less than one percent of the calculated losses and has therefore an effect in the order of magnitude of 10^{-4} on the calculated neutron fluence. This effect can be neglected as it is well within the accuracy of the calculations.
Regarding the correction for the Al window the error made has an average effect of one-tenth of a percent on the fluence result and is equally compatible with the desired accuracy for the fluence of 1 %.

9.2 Experimental data, neutron transmission experiment with air

Table 11: Experimental data of environmental conditions, 3.March 2010.

Time	Atm. Pressure [Bar]	Temperature [°C]	Rel. Atm. Moisture [%]
13:20	1.0221	22.4	23
13:30	1.0222	22.3	23
13:40	1.0218	22.2	23
13:50	1.0215	22.1	23
14:00	1.0213	22.1	23
14:10	1.0213	22	23
14:20	1.0212	22	23
14:30	1.0213	22	24
14:40	1.0213	21.9	24
14:50	1.0210	21.9	24
15:00	1.0208	21.9	24
15:10	1.0207	21.9	23
15:20	1.0206	21.9	23
15:30	1.0205	21.9	23
Mean Value	1.0213 ± 0.0005	22.04 ± 0.16	23.29 ± 0.47

Table 12: Experimental data of neutron monitor, 3.March 2010.

Start Time	Monitor Counts n_m	Measurement Time [s]	Measurement
13:22:24	135430	1200	Vacuum 1
13:46:01	134670	1200	Vacuum 2
14:10:55	135092	1200	Air 1
14:40:35	134190	1200	Air 2
15:07:45	134563	1200	Vacuum 3

Table 13: Experimental Data, 3.March 2010.

Counts $[n/n_m]$ $E_n = 0.12$ eV Air	Counts $[n/n_m]$ $E_n = 0.12$ eV Vacuum	Test Series Number	Counts $[n/n_m]$ $E_n = 0.03$ eV Vacuum	Counts $[n/n_m]$ $E_n = 0.03$ eV Air
0.648 ± 0.003	0.684 ± 0.003	1	1.752 ± 0.005	1.651 ± 0.005
0.663 ± 0.003	0.691 ± 0.003	2	1.758 ± 0.005	1.672 ± 0.005
	0.683 ± 0.003	3	1.753 ± 0.005	
0.656 ± 0.008	0.686 ± 0.004	Mean Value	1.754 ± 0.003	1.662 ± 0.011
(95.54 ± 1.29) %		Transmission	(94.72 ± 0.65) %	

Table 14: Experimental data of environmental conditions, 4.March 2010.

Time	Atm. Pressure [Bar]	Temperature [°C]	Rel. Atm. Moisture [%]
10:40	1.0134	21.1	20
10:50	1.0135	21.1	20
11:00	1.0133	21.2	20
11:10	1.0133	21.2	20
11:20	1.0133	21.3	20
11:30	1.0133	21.3	20
11:40	1.0130	21.3	20
11:50	1.0130	21.3	20
12:00	1.0128	21.3	20
12:10	1.0128	21.4	20
12:20	1.0125	21.4	20
12:30	1.0124	21.4	20
12:40	1.0123	21.4	20
12:50	1.0122	21.4	20
13:00	1.0121	21.4	20
13:10	1.0120	21.6	21
13:20	1.0119	21.6	21
13:30	1.0119	21.6	21
13:40	1.0119	21.5	21
13:50	1.0118	21.4	21
14:00	1.0117	21.4	21
Mean Value	1.0126 ± 0.0006	21.36 ± 0.14	20.29 ± 0.46

Table 15: Experimental data of neutron monitor, 4.March 2010.

Start Time	Monitor Counts n_m	Measurement Time [s]	Measurement
10:44:09	136251	1200	Vacuum 1
11:07:02	136122	1200	Vacuum 2
11:29:10	135680	1200	Air 1
11:52:05	136001	1200	Air 2
12:25:29	135157	1200	Vacuum 3
12:46:27	135222	1200	Vacuum 4
13:12:21	135556	1200	Air 3
13:33:24	135841	1200	Air 4

Table 16: Experimental Data, 4.March 2010.

Counts $[n/n_m]$ $E_n = 0.12$ eV Air	Counts $[n/n_m]$ $E_n = 0.12$ eV Vacuum	Test Series Number	Counts $[n/n_m]$ $E_n = 0.03$ eV Vacuum	Counts $[n/n_m]$ $E_n = 0.03$ eV Air
0.645 ± 0.003	0.675 ± 0.003	1	1.773 ± 0.005	1.662 ± 0.005
0.651 ± 0.003	0.674 ± 0.003	2	1.761 ± 0.005	1.660 ± 0.005
0.652 ± 0.003	0.685 ± 0.003	3	1.765 ± 0.005	1.649 ± 0.005
0.649 ± 0.003	0.681 ± 0.003	4	1.766 ± 0.005	1.648 ± 0.005
0.649 ± 0.003	0.679 ± 0.005	Mean Value	1.766 ± 0.005	1.655 ± 0.007
(95.58 ± 0.83) %		Transmission	(93.72 ± 0.48) %	

Table 17: Experimental data of environmental conditions, 5.March 2010.

Time	Atm. Pressure [Bar]	Temperature [°C]	Rel. Atm. Moisture [%]
10:10	1.0192	20.9	16
10:20	1.0192	20.8	16
10:30	1.0193	20.7	16
10:40	1.0192	20.7	16
10:50	1.0194	20.7	16
11:00	1.0195	20.7	15
11:10	1.0196	20.6	16
11:20	1.0196	20.6	16
11:30	1.0195	20.3	16
11:40	1.0195	20.3	15
11:50	1.0195	20.4	16
12:00	1.0196	21	15
12:10	1.0196	21.6	14
12:20	1.0194	22	14
12:30	1.0193	22.3	13
12:40	1.0195	22.5	13
12:50	1.0194	22.7	13
13:00	1.0192	22.8	13
13:10	1.0190	22.8	13
13:20	1.0189	22.8	13
13:30	1.0189	22.9	13
13:40	1.0190	23.1	13
Mean Value	1.0193 ± 0.0002	21.51 ± 1.03	14.59 ± 1.37

Table 18: Experimental data of neutron monitor, 5.March 2010.

Start Time	Monitor Counts n_m	Measurement Time [s]	Measurement
10:45:36	139926	1200	Vacuum 1
11:10:23	140614	1200	Air 1
11:40:11	139492	1200	Vacuum 2
12:05:56	138750	1200	Air 2
12:37:53	138924	1200	Vacuum 3
13:11:03	138218	1200	Air 3

Table 19: Experimental Data, 5.March 2010.

Counts $[n/n_m]$ $E_n = 0.12$ eV Air	Counts $[n/n_m]$ $E_n = 0.12$ eV Vacuum	Test Series Number	Counts $[n/n_m]$ $E_n = 0.03$ eV Vacuum	Counts $[n/n_m]$ $E_n = 0.03$ eV Air
0.699 ± 0.003	0.731 ± 0.003	1	1.888 ± 0.005	1.773 ± 0.005
0.711 ± 0.003	0.733 ± 0.003	2	1.879 ± 0.005	1.797 ± 0.005
0.710 ± 0.003	0.739 ± 0.003	3	1.884 ± 0.005	1.791 ± 0.005
0.707 ± 0.007	0.734 ± 0.004	Mean Value	1.884 ± 0.005	1.787 ± 0.013
(96.23 ± 1.09) %		Transmission	(94.87 ± 0.74) %	

Table 20: Experimental data of environmental conditions, 9.March 2010.

Time	Atm. Pressure [Bar]	Temperature [°C]	Rel. Atm. Moisture [%]
09:20	1.0249	22.5	13
09:30	1.0249	22.6	13
09:40	1.0248	22.7	13
09:50	1.0249	22.8	13
10:00	1.0249	22.8	13
10:10	1.0250	22.9	13
10:20	1.0250	23	13
10:30	1.0249	23	13
10:40	1.0249	23.1	13
10:50	1.0250	23.1	13
11:00	1.0252	23.1	13
11:10	1.0251	23.1	13
11:20	1.0251	23.1	13
11:30	1.0251	23.1	13
11:40	1.0249	23.1	13
11:50	1.0250	23.1	13
12:00	1.0249	23.1	13
12:10	1.0250	23.1	13
12:20	1.0249	23.1	13
12:30	1.0249	23.2	12
12:40	1.0248	23.2	12
12:50	1.0248	23.2	12
13:00	1.0248	23.2	12
13:10	1.0247	23.2	12
13:20	1.0247	23.2	12
13:30	1.0246	23.2	12
13:40	1.0245	23.2	12
13:50	1.0242	23.3	12
14:00	1.0242	23.3	12
14:10	1.0241	23.3	12
14:20	1.0240	23.3	12
14:30	1.0240	23.3	12
14:40	1.0240	23.3	12
14:50	1.0238	23.3	12
15:00	1.0238	23.3	12
Mean Value	1.0249 ± 0.0004	23.1 ± 0.2	12.54 ± 0.51

Table 21: Experimental data of neutron monitor, 9.March 2010.

Start Time	Monitor Counts n_m	Measurement Time [s]	Measurement
09:23:26	141002	1200	Vacuum 1
10:03:56	139738	1200	Air 1
10:32:13	139476	1200	Vacuum 2
10:56:01	138826	1200	Air 2
11:37:44	138251	1200	Vacuum 3
12:11:35	138760	1200	Air 3
12:42:21	138444	1200	Vacuum 4
13:07:04	138553	1200	Air 4
14:02:39	138455	1200	Vacuum 5
14:30:40	137582	1200	Air 5

Table 22: Experimental Data, 9.March 2010.

Counts $[n/n_m]$ $E_n = 0.12$ eV Air	Counts $[n/n_m]$ $E_n = 0.12$ eV Vacuum	Test Series Number	Counts $[n/n_m]$ $E_n = 0.03$ eV Vacuum	Counts $[n/n_m]$ $E_n = 0.03$ eV Air
0.559 ± 0.003	0.570 ± 0.003	1	1.534 ± 0.005	1.450 ± 0.005
0.569 ± 0.003	0.595 ± 0.003	2	1.519 ± 0.005	1.452 ± 0.005
0.567 ± 0.003	0.598 ± 0.003	3	1.528 ± 0.005	1.439 ± 0.005
0.574 ± 0.003	0.602 ± 0.003	4	1.517 ± 0.005	1.444 ± 0.005
0.578 ± 0.003	0.599 ± 0.003	5	1.515 ± 0.005	1.448 ± 0.005
0.570 ± 0.007	0.593 ± 0.013	Mean Value	1.523 ± 0.008	1.446 ± 0.005
(96.09 ± 2.42) %		Transmission	(94.97 ± 0.59) %	

9.3 Programs, n_TOF data analysis

9.3.1 Collecting experimental TOF data

/* program for collecting experimental data in root file "TOFanalysis.root" */

- analysis() ... creates TOFanalysis.root with histograms hMaster1-hMasterSumme, 1000 bins
- main() .... reads run.root and number of protons of a file and calls addData()
- addData("run_9236.root",7.47e+13,int bins) ... needs runnr., the number of protons and the number of bins; function for main()
- protonen(const char *datei) ... sums the number of protons of the runs, used in main() and addData()

```
#include "TMath.h"
#include "TStopwatch.h"
#include "TTree.h"
#include "TH1.h"
#include "TFile.h"
// ============ function prototypes ============
void analysis();
int main();
void addData(const char *datei, float protons, int bins);
float protonen(const char *datei);
//=============================================
void analysis()
{
int bins = 1000;
TFile *f = new TFile("TOFanalysis.root","RECREATE");

// create and save the Masterhistograms for the 2 detectors and the sum
// experimental data is of type - F : a 32 bit floating point (Float_t)
TH1F *hMaster1 = new TH1F("hMaster1", "Masterhistogramm von Ausgang 1", bins, 3,
8);
// for averaging the data, not summing
hMaster1->SetBit(TH1::kIsAverage);
hMaster1->Write();
TH1F *hMaster3 = new TH1F("hMaster3", "Masterhistogramm von Ausgang 3", bins, 3,
8);
hMaster3->SetBit(TH1::kIsAverage);
hMaster3->Write();
TH1F *hMasterSumme = new TH1F("hMasterSumme", "Masterhistogramm Summe der
Detektoren", bins, 3, 8);
hMasterSumme->SetBit(TH1::kIsAverage);
hMasterSumme->Write();
f->ls(); // show file
```

```
f->Close(); // close file
}
//=============================================
int main()
{
const char runs[20];
char string[50],file[20];
float protons,usedprotons=0;
int i,messungen=0;
int bins=1000;

// user defines the file with all listed run.root files written in
cout«"Datei mit run Informationen:";
cin»runs;
FILE *MyFile = fopen(runs,"r");
TStopwatch timer;
timer.Start();

// Error message
if (MyFile==NULL)perror("Error opening file");
// read the file with information about runs
else{while(fgets(&string,50,MyFile))
{sscanf(&string[0],"%s",&file);
// information for user about the status of the program
cout « "" « endl;
cout « file « endl;
// call protonen
protons = protonen(file);
// call addData
addData(file, protons, bins);
messungen++;
usedprotons = usedprotons + protons;
}
}
cout « "" « endl;
cout « "total number of processed runs = " « messungen « endl;
cout « "total number of protons = " « usedprotons « endl;
fclose(MyFile);

timer.Stop();
std::cout « " runtime " « timer.RealTime() « " " « timer.CpuTime() « std::endl;
return 0;
}
```

9.3.2 Converting TOF to neutron energy

/* program to convert TOF histograms into neutron energy histograms */

- main() ... calculates the neutron energy according to the time-energy calibration for the old target

```
#include "TMath.h"
// ============ function prototypes ============
void main();
//================================================
void main()
{
Double_t toflow,faktor,L,Lneu,einfach;
Double_t entry,sum,error,sumerror;
// array for energyvalues
Double_t energy[1001],energyeinfach[1001];
int i,bins;

TFile f("TOFanalysis.root","update");

bins = hMaster1->GetNbinsX();
cout « bins « " bins in histograms" « endl;

// distance detector to target in meters
L = 183.8;
// see time-energy-calibration.pdf from Bari/Italy
faktor = (72.2977*L)**2;

// calculation of the energyvalues for the new histogram
for(i=0;i<bins+1;i++){
// tof [mikrosec.]
toflow = TMath::Power(10,hMaster1->GetBinLowEdge(i))*1e-3;
// energy [eV] without correction for the non constant flightpath
einfach = faktor / (toflow**2);
energyeinfach[bins-i] = TMath::Log10(einfach);
// time_energy_NIMA2004.pdf time offset t_0 = -68 +/- 13 [ns] equal to DL = (0.094
+/- 0.018)*Sqrt(E) [cm]
// flightpath [m] calculation, energydependent
Lneu = L + (0.094*TMath::Sqrt(einfach))*1e-2;
// correct energy relation [eV]
energy[bins-i] = TMath::Log10((72.2977*Lneu/toflow)**2);
}
// output for user
cout«"highest energy = "«TMath::Power(10,energy[1000])«" eV"«endl;
cout«"lowest energy = "«TMath::Power(10,energy[0])«" eV"«endl;
// creating energy histograms
```

```
TH1F *hEnergy1 = new TH1F("hEnergy1", "Master histogram Det.1 in eV",bins,energy);
// for associated error
hEnergy1->Sumw2();
// for averaging the data, not summing
hEnergy1->SetBit(TH1::kIsAverage);
hEnergy1->Write();
TH1F *hEnergy3 = new TH1F("hEnergy3", "Master histogram Det.3 in eV",bins,energy);
hEnergy3->Sumw2();
hEnergy3->SetBit(TH1::kIsAverage);
hEnergy3->Write();
TH1F *hEnergySumme = new TH1F("hEnergySumme", "Master histogram both detectors in eV",bins,energy);
hEnergySumme->Sumw2();
hEnergySumme->SetBit(TH1::kIsAverage);
hEnergySumme->Write();
// creating histogram for comparison with time-energy calibration
TH1F *hEnergy2 = new TH1F("hEnergysimple", "energy calculated without time-energy-calibration",bins,energyeinfach);
hEnergy2->SetBit(TH1::kIsAverage);
hEnergy2->Write();
// creating flux histograms
TH1F *hFlux1 = new TH1F("hFlux1", "flux histogram for Det. 1, MCNP simulation", bins, energy);
hFlux1->Write();
TH1F *hFlux3 = new TH1F("hFlux3", "flux histogram for Det. 3, MCNP simulation", bins, energy);
hFlux3->Write();
TH1F *hFluxSumme = new TH1F("hFluxSumme", "flux histogram for the sum of the 2 detectors, MCNP simulation", bins, energy);
hFluxSumme->Write();

// loop for filling the energyhistograms with the counts and the associated errors
for(i=0;i<bins;i++){
entry = hMaster1->GetBinContent(i);
error = hMaster1->GetBinError(i);
sum = entry;
sumerror = error;
hEnergy1->SetBinContent(bins-i,entry);
// filling the histogram without time-energy calibration with data of Det.1
hEnergy2->SetBinContent(bins-i,entry);
hEnergy1->SetBinError(bins-i,error);
entry = hMaster3->GetBinContent(i);
error = hMaster3->GetBinError(i);
sum = (sum + entry)/2;
sumerror = (sumerror + error)/2;
hEnergy3->SetBinContent(bins-i,entry);
hEnergy3->SetBinError(bins-i,error);
hEnergySumme->SetBinContent(bins-i,sum);
```

```
hEnergySumme->SetBinError(bins-i,sumerror);
}
f.Write("",TObject::kOverwrite);
f.Close();
}
```

9.3.3 Collecting ENDF data

/* Program for ENDF data collection, puts data into tree, creates histogram, calculates correction for the material; here correction calculation for air is listed as an example */

- createfile() ... creates rootfile
- histogram("1H") ... reads data from isotope.dat files & fills data into tree & creates histogram with the data; for example, 1H.dat file must be in the same directory
- air("luft.root") ... Calculates Exp[-atoms/barn*sigma] for air and writes it into file luft.root
- data(TH1D *myHist, Int_t bins) ... linear regression for the ENDF data, for histogram intervalls without value
- intervalle(Float_t *energy, int bins) ... function for histogram binning like the experimental data in TOFanalysis.root

```
#include <iostream>
#include <string>
using namespace std;
// ============ function prototypes ============
void createfile();
void histogram(const char *rootfile, string isotope);
void air(const char *rootfile);
void data(TH1D *myHist, Int_t bins);
void intervalle(Float_t *energy, int bins);
//=============================================
void createfile(){
const char datei[20];
// user defines name of rootfile
cout«"name of root file to be created: ";
cin»datei;
// create a new ROOT file
TFile *f = new TFile(datei,"RECREATE");
// create a TTree
TTree *tree = new TTree("T","Data from ENDF_VII.0");
f->Write();
f->Close();
}
//=============================================
void histogram(const char *rootfile, string isotope)
{
// read data from an ascii file and fill into existing root file tree
gROOT->Reset();
Double_t energyTot, sigmaTot;
char line[80];

// create strings for inserting isotope name
```

```
string dat = ".dat";
string ene = "Energy";
string sig = "Sigma";
// fill in isotope
dat.insert(0,isotope);
ene.insert(0,isotope);
sig.insert(0,isotope);
// cast strings to const char pointer
const char *datei = dat.c_str();
const char *energy = ene.c_str();
const char *sigma = sig.c_str();

// open the ASCII file
FILE *fp = fopen(datei,"r");
// open existing ROOT file
TFile f(rootfile,"update");
// create branches with information
T->Branch(energy,&energyTot,"energy/D");
T->Branch(sigma,&sigmaTot,"sigma/D");
// fill the tree from the values in ASCII file
while (fgets(&line,80,fp)) {
// values are double => %le !!!
sscanf(&line[0],"%le %le",&energyTot,&sigmaTot);
// as the first lines in data files are comments
if (sigmaTot != 0){
energyTot = energyTot * 1e+6;
T->Fill();
}
}
fclose(fp);
f.Write("",TObject::kOverwrite);
f.Close();
// make histogram
cout«"Histogramm wird erstellt"«endl;
// array for histogram bins
Float_t rtn[1001]={0};
// gets filled with the bins of the experimental data histograms
intervalle(rtn,1001);
Float_t *xbins = rtn;
int bins = 1000;
TFile f1(rootfile,"update");
// create Profilehistogram for dumping the info in
new TProfile("prof","sigma versus Log10(energy)",bins,xbins);
// create the string for the Draw() option
const char word[80];
// "sigma:TMath::Log10(energy)»prof"
strcpy(word,sigma);
// strcat() adds string to string
```

```
strcat(word,":TMath::Log10(");
strcat(word,energy);
strcat(word,")»prof");
// print what is going to be drawn
cout«word«endl;
// make const char pointer to the string for the Draw()
const char *pword = word;
T->Draw(pword);
prof->DrawCopy();
// so that the underflow bin does not get included at the linearisation in ProjectionX()
// otherwise the cross section in the low energy area would be wrong!!!
int i,n;
double content,place;
for(i=1;i<100;i++){
content=prof->GetBinContent(i);
n++;
if(content!=0)break;
}
for(i=0;i<n;i++){
place = prof->GetBinLowEdge(i);
cout«place«endl;
prof->Fill(place,content);
}
// make projection. TProfile::ProjectionX() does not allow to fix the starting bin!!!!
// make 1D Histogramm out of the Profile
TH1D *p = prof->ProjectionX(isotope.c_str(),"e");
// linear regression
data(p,bins);
p->Write();
prof->Delete("*");
cout « isotope « endl;
f1.Write("",TObject::kOverwrite);
f1.Close();
}
//=============================================
void air(const char *rootfile)
{
Float_t rtn[1001]=0;
intervalle(rtn,1001);
Float_t *xbins = rtn;
TFile f(rootfile,"update");
Int_t i, bins;
bins = 1000;
// number of atoms per barn
// molar mass or air [kg/mol]
Double_t M = 28.9644e-3;
// density of air at 23°C, [kg/m^3]
Double_t rho = 1.192;
```

```
// Lenght of the air layer at the experiment, 47 cm = 0.47 [m]
Double_t dL = 0.47;
// rho_(Luft)*x in [atoms/barn]
Double_t Atoms = rho*dL*6.022e+23*1e-28/M;
// mass % of air molekules, number of atoms per molekule accounted for
Double_t perH = 2*1.41e-2/3.;
Double_t perN = 2*77.024e-2;
Double_t perO = (2*20.642e-2+1.41e-2/3.);
Double_t perAr = 0.924e-2;
// pointer to existing histograms with cross section data
TH1D *pHel = (TH1D*)f.Get("H1el");
TH1D *pHcap = (TH1D*)f.Get("H1cap");
TH1D *pNel = (TH1D*)f.Get("N14el");
TH1D *pNcap = (TH1D*)f.Get("N14cap");
TH1D *pNnp = (TH1D*)f.Get("N14np");
TH1D *pOel = (TH1D*)f.Get("O16el");
TH1D *pOcap = (TH1D*)f.Get("O16cap");
TH1D *pAr36el = (TH1D*)f.Get("Ar36el");
TH1D *pAr36cap = (TH1D*)f.Get("Ar36cap");
TH1D *pAr40el = (TH1D*)f.Get("Ar40el");
TH1D *pAr40cap = (TH1D*)f.Get("Ar40cap");
// calculate sigma tot for Argon
TH1D *pAr40 = (TH1D*)f.Get("Ar40tot");
TH1D *pAr36 = (TH1D*)f.Get("Ar36tot");
TH1D *pArtotal = new TH1D("Artotal","sigma total of Argon (40 and 36, weighed)",
bins, xbins);
pArtotal->Sumw2();
pArtotal->Add(pAr40,pAr36,99.6e-2,0.4e-2);
// Histogram for total cross sections with correction for strong binding
TH1D *pH = new TH1D("H","sigma total of Hydrogen", bins, xbins);
pH->Sumw2();
pH->Add(pHel,pHcap,((1+1)/1)**2,1);
TH1D *pN = new TH1D("N","sigma total of Nitrogen", bins, xbins);
pN->Sumw2();
pN->Add(pNel,pNcap,((14+1)/14.)**2,1);
pN->Add(pNnp,1);
TH1D *pO = new TH1D("O","sigma total of Oxygen", bins, xbins);
pO->Sumw2();
pO->Add(pOel,pOcap,((16+1)/16.)**2,1);
TH1D *pAr = new TH1D("Ar","sigma total of Argon", bins, xbins);
pAr->Sumw2();
pAr->Add(pAr36el,pAr36cap,1,1);
// 0.336% 36Ar is nat. present, must be accounted for as sigma(36Ar) is a factor 1e3
bigger; here 0.4% in order to disregard 38Ar
pAr->Scale(0.4e-2);
pAr->Add(pAr40el,99.6e-2);
pAr->Add(pAr40cap,99.6e-2);
//————————————
```

```
// Histogram for the sum of the cross sections, weighed with materials
TH1D *hSum = new TH1D("SumMat","crossection of the sum of all materials in air",
bins, xbins);
hSum->Sumw2();
hSum->Add(pO,pN,perO,perN);
hSum->Add(pArtotal,perAr);
hSum->Add(pH,perH);
// Histogram for correction factor
TH1D *hCorr = new TH1D("Corr","with scattercorr. Factor for 47 cm air", bins, xbins);
hCorr->Sumw2();
//————————————————
// Histogramm for capture only correction
TH1D *hCapture = new TH1D("CorrCapture","capture corr. Factor for 47 cm air", bins,
xbins);
hCapture->Sumw2();
TH1D *hCap = new TH1D("capture","capture cross section all molekules", bins, xbins);
hCap->Sumw2();
hCap->Add(pHcap,pNcap,perH,perN);
hCap->Add(pNnp,perN);
hCap->Add(pOcap,perO);
hCap->Add(pAr36cap,perAr*0.4e-2);
hCap->Add(pAr40cap,perAr*99.6e-2);
//————————————————
// Histogramm for correction factor with pure sigma total of the Mat., ENDF data
TH1D *hOhne = new TH1D("CorrOhne","without scattercorr. Factor for 47 cm air",
bins, xbins);
hOhne->Sumw2();
TH1D *pHtot = (TH1D*)f.Get("H1tot");
TH1D *pNtot = (TH1D*)f.Get("N14tot");
TH1D *pOtot = (TH1D*)f.Get("O16tot");
TH1D *htot = new TH1D("tot","total cross section for air, ENDF all molekules sig. tot.",
bins, xbins);
htot->Sumw2();
htot->Add(pHtot,pNtot,perH,perN);
htot->Add(pOtot,perO);
htot->Add(pArtotal,perAr);
//————————————————
// calculate EXP(-sigma_tot*atoms/barn)
for(i=0; i<bins; i++){
hCorr->SetBinContent(i,TMath::Exp(-(Atoms*hSum->GetBinContent(i))));
hOhne->SetBinContent(i,TMath::Exp(-(Atoms*htot->GetBinContent(i))));
hCapture->SetBinContent(i,TMath::Exp(-(Atoms*hCap->GetBinContent(i))));
}

f.Write("",TObject::kOverwrite);
f.Close();
}
```

9.3.4 Calculation of the reaction yield

/* Program for calculating the reaction yield */

- yield() ... calculates the yield after the series for the multi layer correction and commissioning paper 2004

```
// ============ function prototypes ============
void yield();
void intervalle(Float_t *energy, int bins);
//=============================================
void yield()
{
Float_t rtn[1001]={0};
intervalle(rtn,1001);
Float_t *xbins = rtn;
Double_t Taatoms,Ptatoms,Uatoms,Tawindow;
Int_t i, bins;
// number of histogram bins
bins = 1000;
TFile f("reihe.root","update");

// number of atoms per barn, Tantalum electrodes
Double_t rhoTa = 16.69; // g/cm^3
Double_t MTa = 180.94788; // g/mol
Double_t dTa = 0.0125; // cm
Taatoms = 6.022e23*1e-24*rhoTa*dTa/MTa;
// Tantalum window 15 mm thick
Double_t dTawindow = 0.015; //cm
Tawindow = 6.022e23*1e-24*rhoTa*dTawindow/MTa;
// Platinum electrodes
Double_t rhoPt = 21.45; // g/cm^3
Double_t MPt = 195.084; // g/mol
Double_t dPt = 0.0125; // cm
Ptatoms = 6.022e23*1e-24*rhoPt*dPt/MPt;
// Uranium deposits, U atoms per layer in the fission chamber
Uatoms = 1.13745e-6;

// output for user
cout«"Ta atoms per barn = "«Taatoms«endl;
cout«"Ta atoms per barn in window = "«Tawindow«endl;
cout«"Pt atoms per barn = "«Ptatoms«endl;
cout«"U atoms per barn = "«Uatoms«endl;

// Histograms for yields
TH1D *hYieldReihe = new TH1D("YieldReihe","Yield with corrections from my series",
bins, xbins);
```

```
hYieldReihe->Sumw2();
TH1D *hYieldMultilayer = new TH1D("multilayer","Yield with correction for multi layer
structure, commissioning paper, and materials",bins,xbins);
hYieldMultilayer->Sumw2();
TH1D *hOhnemultilayer = new TH1D("simpleyield","Yield with correction for materials
before first electrode", bins, xbins);
hOhnemultilayer->Sumw2();
// Histograms for corrections
TH1D *hCorrReihe = new TH1D("CorrReihe","Correction from my series", bins, xbins);
hCorrReihe->Sumw2();
TH1D *hCorrTaWindow = new TH1D("Tawindow","Correctionfactor for Ta window",
bins, xbins);
hCorrTaWindow->Sumw2();
TH1D *hanalytisch = new TH1D("analytisch","all corrections from analytical calcula-
tion", bins, xbins);
hanalytisch->Sumw2();
TH1D *hurancap = new TH1D("capturecorr","correction for capture events in first 1/2
of chamber", bins, xbins);
hurancap->Sumw2();
// pointer to histograms with total cross sections and correction factors
TH1D *pTa = (TH1D*)f.Get("Tacap");
TH1D *pPt = (TH1D*)f.Get("Ptcap");
TH1D *pUfis = (TH1D*)f.Get("hUfission");
TH1D *pUcap = (TH1D*)f.Get("hUcapture");
TH1D *pAir = (TH1D*)f.Get("CorrAir");
TH1D *pWindow = (TH1D*)f.Get("CorrAlalloy");

Double_t Ta,TaWindow,Tatotal,Pl,Pltotal,U,Utotal,AlWindow,Air;
Double_t Content,Commissioning,Ohnelayer,meinekorr,analytisch;

for(i=0; i<bins; i++){
// calculating the correction factors EXP(-sigma_tot*atoms/barn)
Ta = TMath::Exp(-Taatoms*pTa->GetBinContent(i));
Tatotal = TMath::Exp(-Taatoms*5*pTa->GetBinContent(i));
Pl = TMath::Exp(-Ptatoms*pPt->GetBinContent(i));
Pltotal = TMath::Exp(-Ptatoms*5*pPt->GetBinContent(i));
U = TMath::Exp(-Uatoms*pUcap->GetBinContent(i));
// commissioning paper
Utotal = TMath::Exp(-Uatoms*10*pUcap->GetBinContent(i)/2.);
TaWindow = TMath::Exp(-Tawindow*pTa->GetBinContent(i));
// correction for multilayer structure
meinekorr = 1/10.*(Ta+Ta*U*Pl)*(1+Ta*U**2*Pl+(Ta*U**2*Pl)**2
+(Ta*U**2*Pl)**3+(Ta*U**2*Pl)**4);
// corrections for the Al windows and air
AlWindow = pWindow->GetBinContent(i);
Air = pAir->GetBinContent(i);
// calculate the yield
```

```
Content = (Air*AlWindow*TaWindow*meinekorr*(1-TMath::Exp(-Uatoms*10
pUfis->GetBinContent(i))));
// commissioning paper
Commissioning = (Air*AlWindow*TaWindow*Utotal*(1-TMath::Exp(-Uatoms*10
pUfis->GetBinContent(i))));
// simple approximation
Ohnelayer = (Air*AlWindow*TaWindow*(1-TMath::Exp(-Uatoms*10
pUfis->GetBinContent(i))));
// calculate corrections
analytisch = Air*AlWindow*TaWindow*meinekorr;
// fill the histograms with the values
hYieldReihe->SetBinContent(i,Content);
hYieldMultilayer->SetBinContent(i,Commissioning);
hOhnemultilayer->SetBinContent(i,Ohnelayer);
hCorrTaWindow->SetBinContent(i,TaWindow);
hCorrReihe->SetBinContent(i,meinekorr);
hanalytisch->SetBinContent(i,analytisch);
hurancap->SetBinContent(i,Utotal);
}

f.Write("",TObject::kOverwrite);
YieldReihe->DrawCopy();
multilayer->SetLineColor(2);
multilayer->DrawCopy("same");
simpleyield->SetLineColor(3);
simpleyield->DrawCopy("same");
f.Close();
}
```

9.3.5 Calculating the neutron fluence

/* Program for calculating the fluence */

- main() ... calculates the flux with yield from MCNP simulation and analytical yield
- linear() ... calculates flux on linear energy scale

```
// ============ function prototypes ============
void main();
void linear();
void intervalle(Float_t *energy, int bins);
//=============================================
void main()
{
Int_t bins = 1000;
Float_t rtn[1001]=0;
intervalle(rtn,1001);
Float_t *xbins = rtn;
Int_t i;
float yield,eff,trans,isolet,air;
float data, flux;
float reihe, ptb, simple;
// efficiency of the fission chamber
eff = 0.9527;

TFile f("TOFanalysis.root","update");
char fall;
cout«"Data of which detector should be processed: ";
cin»fall;
switch(fall)
{
case '1':
TH1F *hData = (TH1F*)f.Get("hEnergy1");
TH1F *hFlux = (TH1F*)f.Get("hFlux1");
cout«"Data of detector 1 gets processed"«endl;
break;
case '3':
TH1F *hData = (TH1F*)f.Get("hEnergy3");
TH1F *hFlux = (TH1F*)f.Get("hFlux3");
cout«"Data of detector 3 gets processed"«endl;
break;
default:
TH1F *hData = (TH1F*)f.Get("hEnergySumme");
TH1F *hFlux = (TH1F*)f.Get("hFluxSumme");
cout«"Data of the sum of the detectors gets processed "«endl;
}
// Histograms for calculated flux in different ways
```

```
TH1F *hReihe = new TH1F("FluxSeries","Flux with yield from my series", bins, xbins);
hReihe->Sumw2();
TH1F *hPTB = new TH1F("FluxPTB","Flux with yield from commissioning paper",
bins, xbins);
hPTB->Sumw2();
TH1F *hSimple = new TH1F("FluxSimple","Flux from simplest approximation, all ma-
terials behind each other", bins, xbins);
hSimple->Sumw2();

TFile f1("TOF_MCNP.root","r");
// Monte Carlo Simulation: Yield and all corrections except air
TH1D *pMCNP = (TH1D*)f1.Get("MCNP");
TFile f2("reihe.root","r");
TH1D *pReihe = (TH1D*)f2.Get("YieldReihe");
TH1D *pPTB = (TH1D*)f2.Get("multilayer");
TH1D *pSimple = (TH1D*)f2.Get("simpleyield");
TH1D *pAir = (TH1D*)f2.Get("CorrAir");

for(i=0;i<bins;i++){
// flux with yield from MCNP
f1.cd();
yield = pMCNP->GetBinContent(i);
f2.cd();
// air was not in the simulation
air = pAir->GetBinContent(i);
f.cd();
data = hData->GetBinContent(i);
// for calculation in isolethargic units
isolet = hData->GetBinWidth(i)*TMath::Ln10();
if(yield > 0){flux = data/(yield*isolet*eff*air);}
else {flux = 0;}
hFlux->SetBinContent(i,flux);
// flux from analytical calculations
f2.cd();
reihe = pReihe->GetBinContent(i);
ptb = pPTB->GetBinContent(i);
simple = pSimple->GetBinContent(i);
f.cd();
if(reihe > 0){hReihe->SetBinContent(i,data/(reihe*isolet*eff));}
else{hReihe->SetBinContent(i,0);}
if(ptb > 0){hPTB->SetBinContent(i,data/(ptb*isolet*eff));}
else{hPTB->SetBinContent(i,0);}
if(simple > 0){hSimple->SetBinContent(i,data/(simple*isolet*eff));}
else {hSimple->SetBinContent(i,0);}
}

f.Write("",TObject::kOverwrite);
hFlux->DrawCopy("hist");
```

```
FluxSeries->SetLineColor(2);
FluxSeries->DrawCopy("same");
FluxPTB->SetLineColor(3);
FluxPTB->DrawCopy("same");
FluxSimple->SetLineColor(4);
FluxSimple->DrawCopy("same");

f.Close();
f1.Close();
f2.Close();
}

//=============================================
void linear()
{
TFile f("TOFanalysis.root","update");
TH1F *hFluxSumme = (TH1F*)f.Get("hFluxSumme");
Float_t binedge[1001];
int i, bins=1000, a = sizeof(binedge);
cout«a«endl;

for(i=0;i<bins+1;i++){
binedge[i] = TMath::Power(10,hFluxSumme->GetBinLowEdge(i));
}
TH1F *MyLinear = new TH1F("linearflux","flux linear;energy;dn/dln(E)/7e12 ppp", bins,
binedge);
Double_t content;
for (i=0;i<bins;i++){
content = hFluxSumme->GetBinContent(i);
MyLinear->SetBinContent(i,content);
}
f.Write("",TObject::kOverwrite);
f.Close();
}
```

9.3.6 Function for adding the data

```
//=============================================
void addData(const char *datei, float protons, int bins)
{
// prepare data of different detector streams in histograms
TFile f("TOFanalysis.root","UPDATE");
TFile f1(datei);
nt_ptbc->Draw("TMath::Log10(PTBCtof)»h1(1000,3,8)",
"PTBCdetn==1 && PTBCamp>32 && PTBCtof<80000000");
nt_ptbc->Draw("TMath::Log10(PTBCtof)»h3(1000,3,8)",
"PTBCdetn==3 && PTBCamp>16 && PTBCtof<80000000");

TH1F *h1 = (TH1F*)gDirectory->Get("h1");
h1->Sumw2();
h1->Scale(7.0e12/protons);
h1->SetBit(TH1::kIsAverage);

TH1F *h3 = (TH1F*)gDirectory->Get("h3");
h3->Sumw2();
h3->Scale(7.0e12/protons);
h3->SetBit(TH1::kIsAverage);

// information for user about program status
cout « " Histogramme wurden erstellt" « endl;
// change to analysis.root
f.cd();
// add Data of the run to the master histograms
hMaster1->Add(h1,1);
hMaster3->Add(h3,1);
hMasterSumme->Add(h1,1);
hMasterSumme->Add(h3,1);
// save the new Masterhistograms (overwrite old ones)
hMaster1->Write("",TObject::kOverwrite);
hMaster3->Write("",TObject::kOverwrite);
hMasterSumme->Write("",TObject::kOverwrite);
// Close Data(run.root) and Master(TOFanalysis.root) file
f1.Close();
f.Close();
}
//=============================================
```

9.3.7 Function for calculating the number of protons per run

```
//=============================================
float protonen(const char *datei)
{
Int_t i,end,n;
Int_t number,events=0;
float intensity,protonen;

TFile f(datei);
// pointer and shared memory for branch EventNumber of run.root files
TBranch *MyNumber = nt_ptbc->GetBranch("EventNumber");
MyNumber->SetAddress(&number);
end = MyNumber->GetEntries();
MyNumber->GetEvent(0);
// comparison for loop
n = number;
// pointer and shared memory for branch PulseIntensity of run.root files
TBranch *MyIntensity = nt_ptbc->GetBranch("PulseIntensity");
MyIntensity->SetAddress(&intensity);
MyIntensity->GetEvent(0);
// number of protons at the first event
protonen = intensity;

for (i=1;i<end;i++){
MyNumber->GetEvent(i);
// if eventnr. changes, the proton intensity gets read out
if (number != n){
events++;
MyIntensity->GetEvent(i);
protonen = protonen + intensity;
n = number; // new comparison value
}
}
// information for user about program status
cout « " Protonenanzahl = " « protonen « endl;
return protonen;
}
//=============================================
```

9.3.8 Function for data linearisation

```
//=================================================
void data(TH1D *myHist, Int_t bins)
{
Double_t value,content,error;
Double_t xlow,xhi,ylow,yhi,ylowerror,yhierror;
Int_t i,n,j;
for(i=0;i<bins;i++){
value = myHist->GetBinContent(i);
// if first histogram value == 0
if(i==0 && value==0){
n = 0;
// search for first value != 0
while(value == 0){
n++;
value = myHist->GetBinContent(i+n);
}
// take error from first value != 0
error = myHist->GetBinError(i+n);
for(j=0;j<n;j++){
myHist->SetBinContent(i+j,value);
myHist->SetBinError(i+j,error);
}
}
// for all values == 0
while(value == 0){
// lower value
ylow = myHist->GetBinContent(i-1);
ylowerror = myHist->GetBinError(i-1);
xlow = myHist->GetBinCenter(i-1);
n = 0;
// search for next value != 0
while(value == 0 && (i+n)<bins){
n++;
value = myHist->GetBinContent(i+n);
}
// if the last values of histogram are 0, value == 0, error == 0
if(value == 0 && (i+n)>(bins-1)){
value = ylow;
for(j=0;j<n;j++){myHist->SetBinContent(i+j,0);}
i = bins;
break;
}
//————————————-
// upper value
yhi = value;
```

```
yhierror = myHist->GetBinError(i+n);
xhi = myHist->GetBinCenter(i+n);
// Linearisation and error calculation
for(j=0;j<n;j++){
content = ylow + (yhi-ylow)/(xhi-xlow)*(myHist->GetBinCenter(i+j)-xlow);
myHist->SetBinContent(i+j,content);
error = ylowerror + (yhierror-ylowerror)*(myHist->GetBinCenter(i+j)-xlow)
/(xhi-xlow);
myHist->SetBinError(i+j,error);
}
}
}
cout«value«" "«n«endl;
}
//================================================
```

9.3.9 Function for histogram binning

```
//=================================================
void intervalle(Float_t *energy, int bins)
{
Float_t value;
int i;
TFile f("TOFanalysis.root","r");
for(i=1;i<bins+2;i++){
value = hEnergy1->GetBinLowEdge(i);
energy[i-1] = value;
}
}
//=================================================
```